


Synaptotagmin 9 Modulates Spontaneous Neurotransmitter Release in Striatal Neurons by Regulating Substance P Secretion

 Michael J. Seibert,^{1,2} Chantell S. Evans,³ Kevin S. Stanley,¹ Zhenyong Wu,¹ and Edwin R. Chapman¹

¹Howard Hughes Medical Institute and Department of Neuroscience, University of Wisconsin–Madison School of Medicine and Public Health, Madison, Wisconsin 53705, ²Neuroscience Training Program, University of Wisconsin–Madison School of Medicine and Public Health, Madison, Wisconsin 53705, and ³Department of Cell Biology, Duke University School of Medicine, Durham, North Carolina 27710

Synaptotagmin 9 (SYT9) is a tandem C2 domain Ca^{2+} sensor for exocytosis in neuroendocrine cells; its function in neurons remains unclear. Here, we show that, in mixed-sex cultures, SYT9 does not trigger rapid synaptic vesicle exocytosis in mouse cortical, hippocampal, or striatal neurons, unless it is massively overexpressed. In striatal neurons, loss of SYT9 reduced the frequency of spontaneous neurotransmitter release events (minis). We delved into the underlying mechanism and discovered that SYT9 was localized to dense-core vesicles that contain substance P (SP). Loss of SYT9 impaired SP release, causing the observed decrease in mini frequency. This model is further supported by loss of function mutants. Namely, Ca^{2+} binding to the C2A domain of SYT9 triggered membrane fusion *in vitro*, and mutations that disrupted this activity abolished the ability of SYT9 to regulate both SP release and mini frequency. We conclude that SYT9 indirectly regulates synaptic transmission in striatal neurons by controlling SP release.

Key words: exocytosis; neuromodulation; neuropeptide; spontaneous neurotransmitter release; synaptic transmission; synaptotagmin

Significance Statement

Synaptotagmin 9 (SYT9) has been described as a Ca^{2+} sensor for dense-core vesicle (DCV) exocytosis in neuroendocrine cells, but its role in neurons remains unclear, despite widespread expression in the brain. This article examines the role of SYT9 in synaptic transmission across cultured cortical, hippocampal, and striatal neuronal preparations. We found that SYT9 regulates spontaneous neurotransmitter release in striatal neurons by serving as a Ca^{2+} sensor for the release of the neuromodulator substance P from DCVs. This demonstrates a novel role for SYT9 in neurons and uncovers a new field of study into neuromodulation by SYT9, a protein that is widely expressed in the brain.

Received Sep. 29, 2022; revised Jan. 5, 2023; accepted Jan. 10, 2023.

Author contributions: M.J.S. and E.R.C. designed research; M.J.S., C.S.E., K.S.S., and Z.W. performed research; M.J.S., C.S.E., K.S.S., and Z.W. analyzed data; M.J.S. and E.R.C. wrote the first draft of the paper; M.J.S. and E.R.C. edited the paper; M.J.S. and E.R.C. wrote the paper; E.R.C. contributed unpublished reagents/analytic tools.

This work was supported by National Institutes of Health Grants MH061876 and NS097362 to E.R.C. C.S.E. was supported in part by a PhRMA Foundation predoctoral fellowship and University of Wisconsin–Madison Molecular and Cellular Pharmacology Training Grant T32 GM008688. E.R.C. is an Investigator of the Howard Hughes Medical Institute. This article is subject to HHMI's Open Access to Publications policy. HHMI laboratory heads have previously granted a nonexclusive CC BY 4.0 license to the public and a sublicensable license to HHMI in their research articles. Pursuant to those licenses, the author-accepted manuscript of this article can be made freely available under a CC BY 4.0 license immediately upon publication. The data that support the findings of this study are available from the corresponding author upon reasonable request. We thank members of the E.R.C. laboratory and Kathryn Bjornson for insightful comments and valuable discussion related to the manuscript; Devin Larson and Christina Greer for maintaining the mouse colonies used for this research; Marina Caliendo for generating the full-length SYT9 Ca^{2+} ligand mutant constructs; and Wynnie Nguyen for generating the purified recombinant full-length SYT9.

The authors declare no competing financial interests.

Correspondence should be addressed to Edwin R. Chapman at chapman@wisc.edu.

<https://doi.org/10.1523/JNEUROSCI.1857-22.2023>

Copyright © 2023 the authors

Introduction

The synaptotagmins (SYTs) are a large family of membrane trafficking proteins; 17 isoforms have been identified in mammals, each encoded by a distinct gene (Craxton, 2010; Wolfes and Dean, 2020). In addition, most isoforms are thought to undergo alternative splicing, generating further potential diversity within this family (Craxton, 2010). Most isoforms have a single N-terminal transmembrane domain with a short intraluminal domain. In all isoforms, the cytoplasmic domain largely comprises tandem C2 domains that are connected by a short linker. In at least 8 of the 17 isoforms, the C2 domains serve as Ca^{2+} -dependent anionic lipid binding motifs (Rickman et al., 2004; Bhalla et al., 2008). Ca^{2+} binding is thought to be mediated by acidic side chains in two flexible loops that protrude from each C2 domain (R. B. Sutton et al., 1995). In the case of SYT1, Ca^{2+} triggers the partial penetration of these loops into lipid bilayers and facilitates interactions with SNARE proteins (Chapman, 2008).

A current goal is to understand the functional diversity within the SYT family of proteins. SYT1 and SYT2 have been heavily studied and shown to serve as Ca^{2+} sensors that trigger rapid, synchronous synaptic vesicle (SV) exocytosis in neurons (Geppert et al., 1994; Pang et al., 2006a). Importantly, SYT1 and SYT2 form a closely related clade with one more family member, synaptotagmin (SYT9) (Rickman et al., 2004). This homology prompted the idea that SYT9 might also function as a fast Ca^{2+} sensor for SV exocytosis, which is a point we address in detail in the current study. For clarity, we note that SYT9 is sometimes referred to as SYT5, and vice versa; the SYT9 studied here comprises 386 residues (NCBI Gene accession #53420), whereas SYT5 is 491 residues in length (NCBI Gene accession #60510).

Along with SYT1, SYT9 coregulates catecholamine secretion from dense-core vesicles (DCVs) in PC12 cells (Fukuda et al., 2002; Lynch and Martin, 2007). SYT9 also regulates the release of follicle-stimulating hormone from DCVs in the gonadotrophs of female mice in a sex-specific manner (Roper et al., 2015). However, while SYT9 is widely expressed in the brain (Mittelstaedt et al., 2009) (these authors referred to SYT9 as SYT5), its function in neurons remains controversial. One report concluded that SYT9 serves as a Ca^{2+} sensor for rapid SV exocytosis in cultured striatal neurons (Xu et al., 2007). In contrast, SYT9 failed to support SV exocytosis in *Syt1* KO hippocampal neurons, and pHluorin-tagged SYT9 underwent regulated exocytosis in both axons and dendrites of hippocampal neurons, with kinetics suggestive of DCV fusion (Dean et al., 2012).

To address and clarify the function of SYT9 in neurons, we studied synaptic transmission in cultured hippocampal, cortical, and striatal neurons obtained from *Syt9* KO mice; for completeness, *Syt1* KO neurons were examined in parallel. We show that all three classes of neurons express both SYT9 and SYT1, but loss of SYT9 had no discernable effect on evoked neurotransmitter release, while loss of SYT1 disrupted rapid transmission in all three neuronal preparations. SYT9 was able to rescue the loss of synchronous release that is characteristic of *Syt1* KO neurons, but only when overexpressed by ~25-fold, which matched the expression levels of endogenous SYT1. Interestingly, loss of SYT9 in cultured striatal neurons resulted in a specific and unexpected phenotype: a decrease in the spontaneous SV fusion rate (i.e., mini frequency). We then discovered that SYT9 was colocalized with substance P (SP), a DCV peptide hormone known to be enriched in striatal neurons. Moreover, loss of SYT9 impaired action potential (AP)-triggered SP release. Importantly, in patch-clamp experiments, supplementing the bath with this neuropeptide rescued the mini phenotype. Moreover, the structural elements of SYT9 that underlie Ca^{2+} -triggered membrane fusion *in vitro* also support evoked SP release and spontaneous SV fusion in living striatal neurons. These findings reveal a mechanism in which SYT9 indirectly regulates spontaneous transmission in striatal neurons by directly regulating secretion of the neuromodulator, SP.

Materials and Methods

Animals. All neuronal cultures were prepared from early postnatal (P0–P1) mice of either sex in accordance with all relevant regulations and the approval of the University of Wisconsin Institutional Animal Care and Use Committee. Conditional *Syt9* KO mice were obtained from The Jackson Laboratory (Xu et al., 2007). These conditional *Syt9* KO mice were terminally crossed with an E2a-CRE mouse (The Jackson Laboratory) to yield a population of constitutive *Syt9* KO mice; the mice used in this study are all products of this constitutive *Syt9* KO mouse.

Syt1 cKO (conditional KO) mice were a gift from W. Thoreson, (University of Nebraska–Lincoln) (Quadros et al., 2017).

Genotyping. The *Syt9* KO mouse line was maintained as heterozygous breeders so that offspring WT and KO littermates could be studied. To genotype the neonatal pups, tissue samples were taken by collecting ~2 mm of the end of the tail and extracting DNA from the tissue sample using the Kapa Express Extract Kit (Kapa Biosystems). The extracted DNA was then subjected to PCR using in-house designed primers to identify WT and KO alleles. The primers used to identify the WT allele yield a 209 bp amplicon: forward-primer 5'-GCGTCAATGGGAGGAGAGGTCA-3'; reverse-primer 5'-GTCCACTAGGGCTAGCCAGG-3'. The primers used to identify the KO allele yield a 301 bp amplicon: forward-primer 5'-CAGTAGGGAGCGAGCAGAAATATAAAT-3'; reverse-primer 5'-AACTTCGTCGATCGACCTCGAATAA-3'. The PCR product was subjected to agarose gel electrophoresis and imaged on a ChemiDoc MP imaging system (Bio-Rad).

Molecular biology and lentiviral preparation. Lentiviral vectors were based on FUGW (FUGW was a gift from David Baltimore [Addgene plasmid #14883; <https://www.addgene.org/14883/>; RRID:Addgene_14883]) (Lois et al., 2002). The pFUGW vector was modified by substituting the ubiquitin promoter with the human synapsin I promoter (Kügler et al., 2003); this vector is henceforth referred to as pFSynW. pH-SYT9 was generated by replacing SYT1 in pHluorin-SYT1 (a gift from J. Rothman, Yale University) (Fernández-Alfonso et al., 2006) with a SYT9 cDNA (a gift from M. Fukuda, Tohoku University) (Haberman et al., 2003) using PCR splicing via overlap extension. The pHluorin-SYT9 cassette replaced GFP in the cloning site of the pFSynW vector via In-Fusion Cloning (Takara Bio). The SP-pH construct was generated by PCR splicing via overlap extension and comprised the following: the first 68 residues of mouse preprotachykinin, a GS(GSS)₄ linker and a super-ecliptic pHluorin (Miesenböck et al., 1998). This fusion construct was subcloned into pFSynW.

SYT9 Ca^{2+} ligand mutant (CLM) constructs correspond to D-to-N substitutions of two Ca^{2+} ligands in each C2 domain as follows: C2A_mB; D197N and D199N; C2A_mB_m; D330N and D332N. All four mutations are present in the C2A_mB_m construct. These constructs were made by performing site-directed mutagenesis on the *Syt9* cDNA with the QuikChange Lightning Site-Directed Mutagenesis Kit (Agilent Technologies). Full-length CLM constructs were subcloned into pFSynW and used for the rescue experiments in Figure 14, and isolated C2 domain CLM constructs were subcloned into pGEX and used for experiments in Figure 13. cDNA for SNAP-25B was provided by M. C. Wilson (University of New Mexico School of Medicine), and full-length synaptobrevin 2 (SYB2) and syntaxin 1A (SYX) were provided by J. Rothman (Yale University); these SNARE proteins were subcloned into pTrcHis vectors to yield His₆-tagged proteins (Evans et al., 2015).

Cell culture, transient transfection, and lentiviral transduction. Cortical, hippocampal, and striatal regions were obtained by microdissection and kept in ice-cold Hibernate-A (BrainBits) with 2% B-27 until completion of dissection. Neural tissue was then incubated with 0.25% trypsin-EDTA (Corning) for 25 min at 37°C. The tissue was washed with DMEM (Invitrogen) supplemented with FBS (Atlanta Biologicals) and penicillin-streptomycin (Thermo Scientific) and triturated 10–15 times with a P1000 pipette tip until complete dissociation of the tissue. Cells were plated at a density of 100,000 cells/cm² onto poly D-lysine-coated glass coverslips. Supplemented DMEM was replaced after 1 h with Neurobasal-A (Invitrogen) supplemented with B-27 (Thermo Scientific) and GlutaMAX (Thermo Scientific). For SP-pH release experiments, sparse transfection of SP-pH and a cytosolic mRuby marker was required for identifying and imaging single neurons. This was achieved using Lipofectamine LTX with PLUS reagent (Invitrogen) on DIV 8–9. For localization studies, rescue experiments, and Ca^{2+} imaging, full coverage was desirable and was achieved via lentiviral transduction. Lentivirus encoding CRE-recombinase was added to *Syt1* cKO neurons at DIV 0–2, and lentiviruses that expressed SYT9 rescue constructs, the Ca^{2+} imaging construct synaptophysin (SYP)-HaloTag (SYP-Halo) (Bradberry and Chapman, 2022), or SP-pH for localization studies, were added to neurons at DIV 5–7.

Electrophysiological studies. Whole-cell voltage-clamp recordings of cultured neurons (DIV 14–18) were performed at room temperature in

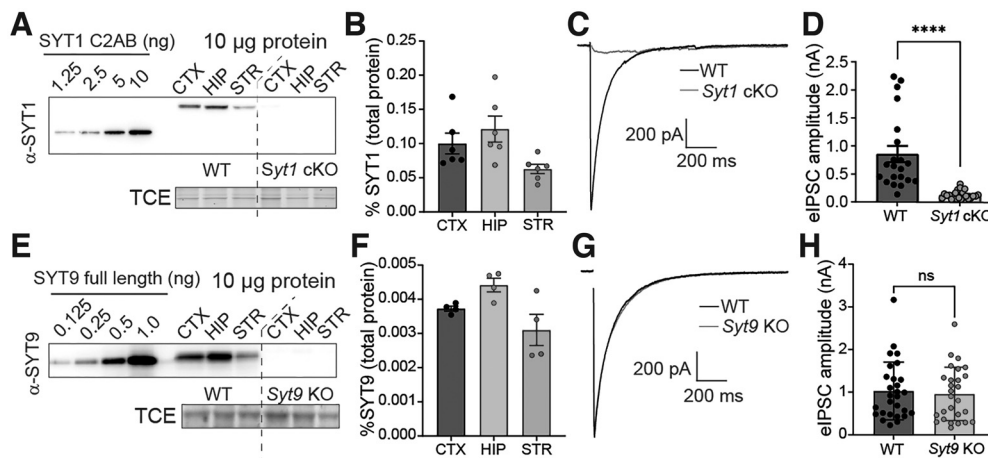


Figure 1. SYT9 is expressed in cultured cortical, hippocampal, and striatal neurons but does not support evoked neurotransmitter release. **A**, Immunoblot of DIV 14 cortical (CTX), hippocampal (HIP), and striatal (STR) neuronal lysates from *Syt1* cKO neurons \pm CRE virus; recombinant SYT1 C2AB served as a standard to quantify SYT1 expression levels. TCE staining served as a loading control. **B**, Quantification of the SYT1 expression levels in each of the three neuronal lysates, as a fraction of total protein ($n = 6$ neuronal preparations). Results are mean \pm SEM: CTX = $0.100 \pm 0.0152\%$, HIP = $0.121 \pm 0.0190\%$, STR = $0.628 \pm 0.00687\%$. **C**, Averaged eIPSC traces from *Syt1* cKO striatal neurons \pm CRE. **D**, Peak eIPSC amplitudes from $-$ CRE ($n = 21$ neurons; 0.854 ± 0.145 nA) or $+$ CRE ($n = 22$ neurons; 0.126 ± 0.0156 nA) neurons, showing loss of synchronous release on loss of SYT1 ($p < 0.0001$; Mann–Whitney $U = 9$). **E**, Same as in **A**, but blotting for SYT9 in lysates from WT and *Syt9* KO striatal neurons, using the indicated amounts of a full-length recombinant SYT9 standard. **F**, Same as in **B**, but for SYT9 expression in WT and *Syt9* KO striatal neurons ($n = 4$). Results are mean \pm SEM: CTX = $0.00373 \pm 0.0000714\%$, HIP = $0.00442 \pm 0.000198\%$, STR = $0.00310 \pm 0.000452\%$; SYT9 is expressed at ~ 25 -fold lower levels than SYT1. **G**, **H**, Same as in **C**, **D**, but in WT ($n = 28$ neurons; 1.03 ± 0.128 nA) and *Syt9* KO ($n = 27$ neurons; 0.959 ± 0.121 nA) striatal neurons. In sharp contrast to *Syt1* cKO $+$ CRE neurons, loss of SYT9 did not affect single eIPSCs in striatal neurons ($p = 0.6979$; unpaired Student's t test $t = 0.3903$, $df = 53$). **** $p < 0.0001$. ns, $p > 0.05$. For all figures, error bars indicate SEM.

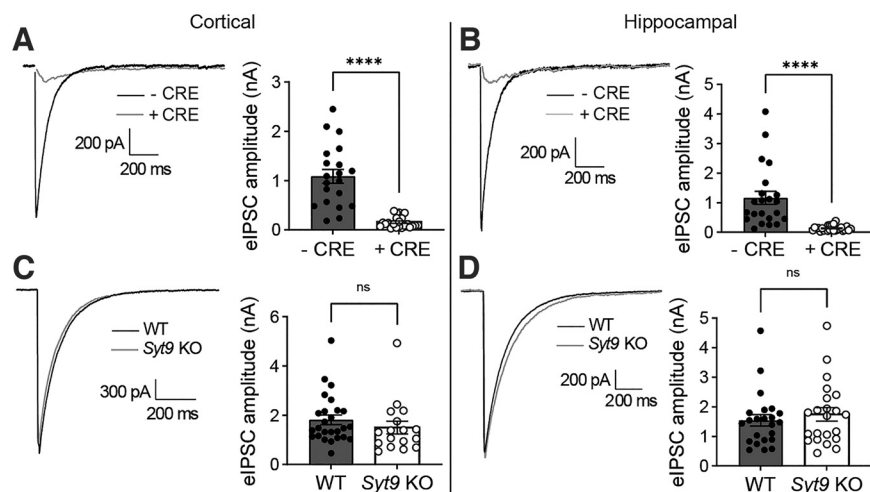


Figure 2. SYT1, but not SYT9, supports evoked neurotransmitter release in cortical and hippocampal neurons. **A**, Averaged eIPSC traces recorded from *Syt1* cKO cortical neurons with quantification of peak eIPSC amplitude $-$ CRE ($n = 20$; 1.09 ± 0.141 nA) and $+$ CRE ($n = 23$; 0.158 ± 0.0237 nA). **B**, Same as in **A**, but with hippocampal neurons ($-$ CRE $n = 22$; 1.16 ± 0.221 nA; $+$ CRE $n = 26$; 0.131 ± 0.0170 nA). **C**, **D**, Same as in **A**, **B**, but using *Syt9* KO neurons; cortical neurons (WT $n = 26$; 1.81 ± 0.193 nA; KO $n = 17$; 1.50 ± 0.225 nA); hippocampal neurons (WT $n = 23$; 1.54 ± 0.192 nA; KO $n = 22$; 1.74 ± 0.226 nA). eIPSCs were disrupted in *Syt1* cKO $+$ CRE cortical ($p < 0.0001$; unpaired t test $t = 6.96$, $df = 41$) and hippocampal neurons ($p < 0.0001$; unpaired t test $t = 5.07$, $df = 46$). In contrast, eIPSCs were unaffected in *Syt9* KO cortical ($p = 0.3231$; unpaired t test $t = 1.000$, $df = 41$) and hippocampal neurons ($p = 0.4966$; unpaired t test $t = 0.686$, $df = 43$).

ACSF containing the following (in mM): 128 NaCl, 5 KCl, 1.5 CaCl₂, 1 MgCl₂, 30 glucose, 25 HEPES, pH 7.4, with an internal solution containing the following (in mM): 130 KCl, 10 HEPES, pH 7.4, 1 EGTA, 2 ATP, 0.3 GTP, 5 phosphocreatine. Recordings were performed using a MultiClamp 700B amplifier and Digidata 1550B digitizer (Molecular Devices) under the control of Clampex 10 software (Molecular Devices). GABA_A-mediated currents were pharmacologically isolated using 20 μ M CNQX (Tocris Bioscience) and 50 μ M D-AP5 (Tocris) in the bath solution; for mIPSC recordings, 1 μ M TTX (Tocris) was included in the bath; 5 mM QX 314 chloride (Tocris) was included in the pipette solutions for

all recordings. Neurons were held at -70 mV in all experiments without correction for liquid junction potentials. Recordings were discarded if series resistance rose above 15 M Ω . For evoked recordings, a concentric bipolar electrode (FHC) was placed 100–200 μ m away from the patched soma, and stimulation currents were adjusted to evoke maximal responses. For mIPSC recordings, 300 s of data was recorded for each striatal neuron, and 180 s of data was acquired for cortical and hippocampal neurons. mIPSCs were quantified for each recording using a template-matching algorithm in Clampfit (Molecular Devices). For pharmacology rescue experiments, SP (Tocris), GR73632 (Tocris), Leu-enkephalin (Tocris), dynorphin A (Tocris), and cholecystokinin (Tocris) were added to the ACSF at 100 nM, and SR140333 (Tocris) was added at 10 nM. Neurons were treated with peptides or drugs for 10 min before patch-clamp experiments were conducted.

Immunoblotting. Coverslips of cultured neurons (DIV 14–18) were rinsed 1–2 times in PBS and lysed by repeated pipetting of lysis buffer (2% SDS, 0.1% Triton X-100, 10 mM EDTA) containing a protease inhibitor cocktail (cComplete mini EDTA-free, Roche). For quantitative Western blots of lysates, protein concentration was determined using a bicinchoninic acid assay (Thermo Scientific) to ensure equal amounts of protein were subjected to SDS-PAGE. Samples were then combined with 4 \times Laemmli sample buffer, heated to 50°C for 15 min, and stored at -20°C until use. For each immunoblot experiment, the samples were subjected to SDS-PAGE on 13% polyacrylamide gels containing 1% trichloroethanol (TCE). After electrophoresis, the TCE was activated by exposure to UV light (300 nm) for 45 s, and labeled proteins were detected via 300 nm illumination; these signals served as a protein loading control (Ladner et al., 2004). Proteins were transferred to a PVDF membrane, which was then blocked with 5% nonfat milk in TBS plus 0.1% Tween 20 (TBST) for 1 h, followed by incubation with primary antibody overnight

at 4°C. Blots were then washed 3 times for 5 min in TBST, incubated with secondary antibody for 1 h, and washed again as above. For the pH-SYT9 rescue experiments, after blotting for SYT9, the PVDF membranes were stripped using Restore Western Blot Stripping Buffer (Thermo Scientific), and the membranes were once again blocked and subsequently probed for SYT1. Primary antibodies were as follows: α -SYT1 (1:500) (DSHB; #mAB 48; RRID:AB_2199314) and α -SYT9 (1:500) (Synaptic Systems catalog #105053, RRID:AB_2199639). Secondary antibodies were goat α -mouse IgG-HRP (Bio-Rad, 1706516; RRID:AB_11125547), goat α -mouse IgG2b-HRP (Invitrogen, M32407; RRID:AB_2536647), and goat α -rabbit IgG-HRP (Bio-Rad, 1706515, RRID:AB_11125142). Immunoreactive bands were visualized using SuperSignal West Pico Plus Chemiluminescent Substrate (Thermo Scientific) and imaged with an GE HealthcareImager 680 imaging system (GE Healthcare). Bands were analyzed by densitometry, with care to stay within the linear range, and contrast was linearly adjusted for publication using ImageJ (Fiji) (Schindelin et al., 2012).

Immunocytochemistry and confocal microscopy. Immunocytochemistry was conducted as previously described (Courtney et al., 2019). For the pH-SYT9 rescue experiments, immediately before fixation and permeabilization, cortical neurons were incubated in primary antibody directed against the pHluorin tag of pH-SYT9 (1:250) (α -GFP; Abcam catalog #ab290, RRID:AB_303395) in culture medium to label only the surface-resident pH-SYT9, as the antibody is unable to enter intact, live neurons. Unbound antibody was removed by washing, and then cells were fixed and permeabilized and incubated a second time with primary antibodies to label SYP (1:1000) (α -SYP; Synaptic Systems catalog #101004; RRID:AB_1210382) and pHluorin (1:1000) (α -GFP; Abcam catalog #ab13970, RRID:AB_300798). This second α -GFP antibody “blocking” antibody, to reveal the internal fraction of pH-SYT9. This strategy allowed for differential secondary labeling of the different pH-SYT9 populations with species-specific secondary antibodies.

Images were acquired on a Zeiss LSM 880 laser scanning confocal microscope with a 63 \times Plan-Apochromat 1.4 NA DIC oil immersion objective. Identical laser and gain settings were used for all samples within each experimental paradigm. Primary antibodies were as follows: α -GFP (1:1000) (Abcam catalog #ab290, RRID:AB_303395), α -GFP (1:1000) (Abcam catalog #ab13970, RRID:AB_300798), α -SYT1 (1:500) (DSHB; #mAB 48; RRID:AB_2199314), α -SYP (1:1000) (Synaptic Systems catalog #101004; RRID:AB_1210382), α -SYT9 (1:500) (Synaptic Systems catalog #105053, RRID:AB_2199639), α -chromogranin B (α -CHGB) (Synaptic Systems catalog #259103; RRID:AB_2619973), α -VGAT (1:1000) (Synaptic Systems catalog #131004; RRID:AB_887873), α -Gephyrin (1:1000) (OriGene catalog #TA502313, RRID:AB_11126039), and α -MAP2 (1:500) (Abcam catalog #ab5392, RRID:AB_2138153). Secondary antibodies were as follows: goat anti-chicken IgY-AlexaFluor-405 (1:500) (Abcam; ab175675, RRID:AB_2810980), goat α -chicken IgY-AlexaFluor-488 (1:500) (Fisher Scientific A-11039, RRID:AB_2534096), goat α -guinea pig IgG-AlexaFluor-488 (1:500) (Fisher Scientific; A-11073; RRID:AB_2534117), goat α -rabbit IgG-AlexaFluor-546 (1:500) (Fisher Scientific; A-11010, RRID:AB_2534077), goat α -guinea pig IgG-AlexaFluor-647 (1:500) (Fisher Scientific; A-11074, RRID:AB_2534118), and goat α -mouse IgG2b-AlexaFluor-647 (1:500) (Fisher Scientific; A-21242; RRID:AB_2535811).

Live-cell imaging. DIV 14–18 striatal neurons were washed twice in ACSF before being mounted in an imaging chamber with parallel platinum electrodes (Warner Instruments) with 500 μ L of ACSF. Imaging was conducted with a 40 \times , 1.4 NA oil-immersion objective on an inverted epifluorescence microscope (IX81, Olympus) equipped with a CMOS camera (Orca Flash 4.0 version 2, Hamamatsu Photonics), motorized stage (Mad City Labs), and a custom illumination source containing three LEDs (470, 530, 625 nm) (Thorlabs). The system was controlled using Micro-Manager (Edelstein et al., 2010). Stimulation was delivered with a stimulation box (SD9, Grass Instrument) controlled via a HEKA EPC10 DAQ-amplifier and PatchMaster software (HEKA), which was also used to synchronize the start of image sequence acquisition. Images were collected using 2 \times 2 binning (0.325 μ m \times 0.325 μ m pixel size).

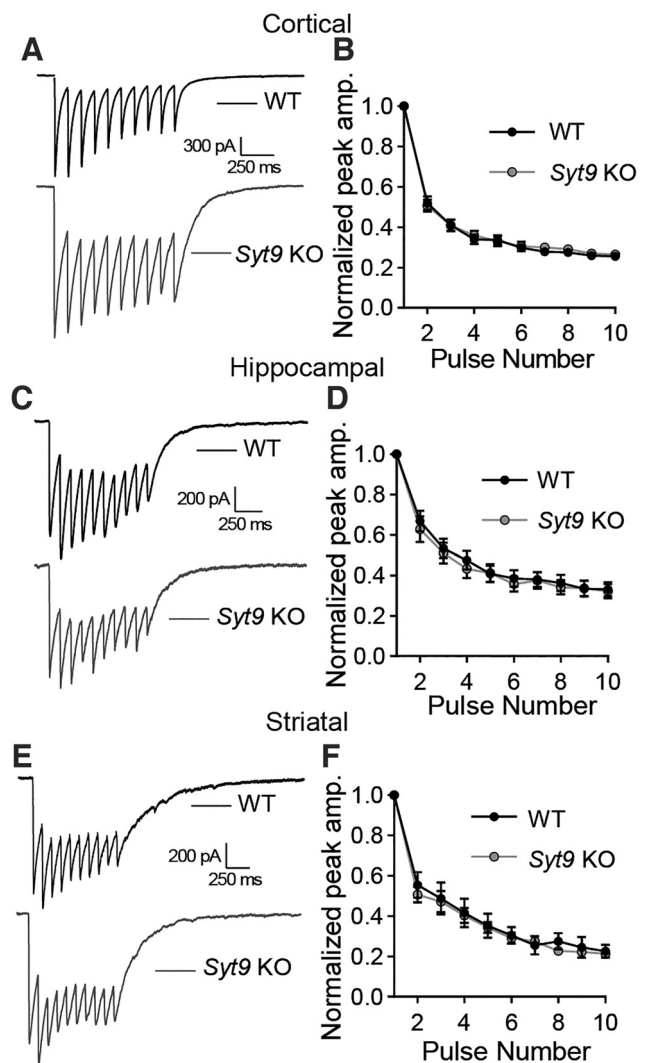


Figure 3. Synaptic depression was unchanged in *Syt9* KO cortical, hippocampal, and striatal neurons. **A**, Averaged 10 Hz eIPSC traces from WT ($n = 21$) and *Syt9* KO ($n = 21$) cortical neurons. **B**, Quantification of peak amplitudes from each pulse normalized to the first pulse, showing no difference in short-term plasticity (multiple unpaired t tests $p > 0.4$). **C**, **D**, Same as in **A**, **B**, but with hippocampal neurons (WT $n = 17$; KO $n = 17$; multiple unpaired t tests $p > 0.5$). **E**, **F**, Same as in **A**, **B**, but with striatal neurons (WT $n = 35$; KO $n = 38$; multiple unpaired t tests $p > 0.2$).

For SP-pH release imaging, an exposure time of 100 ms was used. Neurons were sparsely cotransfected with the SP-pH construct and a cytosolic mRuby construct. Individual transfected neurons were identified for imaging by first detecting the cytosolic mRuby signal with the 530 nm LED and standard RFP filter set (49004, Chroma); this cytosolic mRuby construct also allowed us to ensure that no overlap with other cells was present in the imaging field, ensuring single-cell analysis. SP-pH release was imaged with the 470 nm LED, a standard GFP filter set (49002, Chroma). Ten seconds of baseline were obtained before stimulation was given—16 trains of 50 APs at 50 Hz with 0.5 s between each train. Seventy seconds after the start of stimulation, 500 μ L of 2 \times NH_4Cl ACSF, containing the following (in mM): 100 NH_4Cl , 28 NaCl, 5 KCl, 1.5 CaCl_2 , 1 MgCl_2 , 30 glucose, 25 HEPES, pH 7.4, was added to dequench pHluorin fluorescence to visualize the total number of SP-pH-bearing vesicles.

For Ca^{2+} imaging, the 625 nm LED, custom three-band pass dichroic mirror (Chroma) and far-red emission filter, and a 10 ms exposure time were used. DIV 14–18 striatal neurons that were transduced with a virus that induced expression of SYP-Halo were first washed twice in ACSF before being incubated in ACSF containing 100 nM of the acetoxymethyl

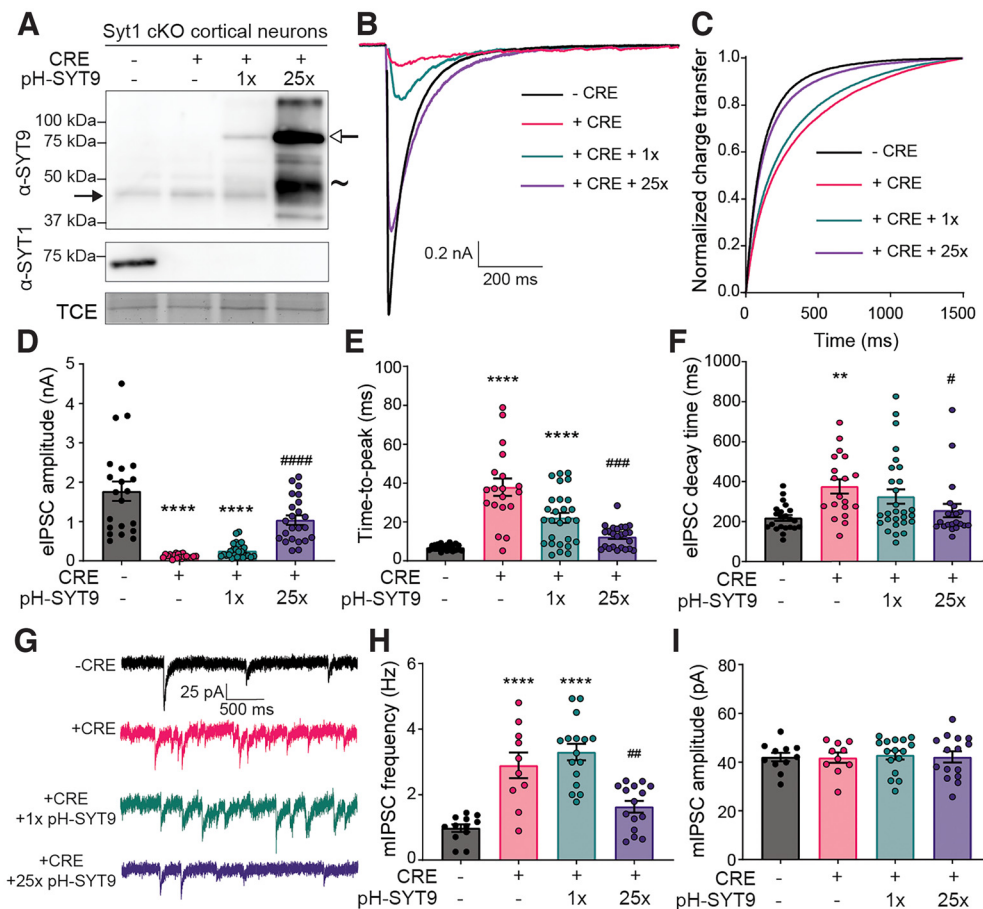


Figure 4. SYT9 rescues *Syt1* KO phenotypes only when overexpressed. **A**, Immunoblots of DIV14 cortical neuronal lysates from *Syt1* cKO mice, \pm CRE lentivirus. TCE staining served as a loading control (in all trials, the α -SYT9 blot was stripped and reprobed with an α -SYT1 antibody, so TCE control is shown only once). + CRE neurons were later transduced with lentivirus encoding pHluorin-tagged SYT9 (pH-SYT9), resulting in either a 1 \times or 25 \times degree of overexpression compared with endogenous SYT9. Closed arrowhead indicates endogenous SYT9. Open arrowhead indicates pH-SYT9. \sim indicates proteolytic fragments from pH-SYT9. **B**, Averaged eIPSC traces recorded from *Syt1* cKO cortical neurons – CRE ($n = 21$ neurons), + CRE ($n = 19$), + CRE + 1 \times pH-SYT9 ($n = 25$), or + CRE + 25 \times pH-SYT9 ($n = 23$). **C**, Plot of normalized cumulative charge transfer of – CRE, + CRE, + CRE + 1 \times pH-SYT9, and + CRE + 25 \times pH-SYT9 conditions. **D**, Average eIPSC amplitudes from **B**. Results are mean \pm SEM: – CRE = 1.773 ± 0.246 nA, + CRE = 0.122 ± 0.0114 nA, + CRE + 1 \times pH-SYT9 = 0.257 ± 0.0375 nA, + CRE + 25 \times pH-SYT9 = 1.035 ± 0.119 nA (Kruskal–Wallis test $H = 64.41$, $p < 0.0001$). Subsequent pairwise analyses with Dunn’s multiple comparisons test resulted in significant p values for – CRE versus + CRE ($p < 0.0001$), – CRE versus + CRE + 1 \times pH-SYT9 ($p < 0.0001$), and + CRE versus + CRE + 25 \times pH-SYT9 ($p < 0.0001$); all other comparisons yielded $p > 0.5$. **E**, Time to peak for each above condition. Results are mean \pm SEM: – CRE = 6.90 ± 0.329 ms, + CRE = 37.9 ± 4.44 ms, + CRE + 1 \times pH-SYT9 = 12.5 ± 1.19 ms (Kruskal–Wallis test $H = 41.41$, $p < 0.0001$). Subsequent pairwise analyses with Dunn’s multiple comparisons test resulted in significant p values for – CRE versus + CRE ($p < 0.0001$), – CRE versus + CRE + 1 \times pH-SYT9 ($p < 0.0001$), and + CRE versus + CRE + 25 \times pH-SYT9 ($p = 0.0003$); all other comparisons yielded $p > 0.1$. SYT9 partially rescued eIPSC amplitude and time to peak, but only when overexpressed 25-fold. **F**, Plot of mean decay time (90%–10%) for each condition. Results are mean \pm SEM: – CRE = 218 ± 14.2 ms, + CRE = 361 ± 40.6 ms, + CRE + 1 \times pH-SYT9 = 325 ± 36.5 ms, + CRE + 25 \times pH-SYT9 = 256 ± 32.9 ms (Kruskal–Wallis test $H = 14.93$, $p = 0.0019$). Subsequent pairwise analyses with Dunn’s multiple comparisons test resulted in significant p values for – CRE versus + CRE ($p = 0.0024$) and + CRE versus + CRE + 25 \times pH-SYT9 ($p = 0.0134$); all other comparisons yielded $p > 0.1$. Further decay analysis was not performed because of receptor-dominated decay kinetics of IPSCs in cultured neurons. **G**, Representative mIPSC traces recorded from the above conditions. **H**, Average mIPSC frequency of each condition showing increased rates of mIPSCs in *Syt1* cKO + CRE ($n = 10$; 2.89 ± 0.392 Hz) neurons compared with – CRE ($n = 12$; 0.976 ± 0.115 Hz). 1 \times overexpression of SYT9 was without effect ($n = 16$; 3.30 ± 0.250 Hz); rescue of the unclamped phenotype was observed at 25 \times overexpression ($n = 15$; 1.63 ± 0.178 Hz) (one-way ANOVA $F = 20.65$, $R^2 = 0.5584$, $p < 0.0001$). Subsequent pairwise analyses with Sidak’s multiple comparisons test resulted in significant p values for – CRE versus + CRE ($p < 0.0001$), – CRE versus + CRE + 1 \times pH-SYT9 ($p < 0.0001$), and + CRE versus + CRE + 25 \times pH-SYT9 ($p = 0.0042$); all other comparisons yielded $p > 0.1$. **I**, mIPSC amplitudes were unchanged across condition (one-way ANOVA $F = 0.0573$, $R^2 = 0.00357$, $p = 0.982$). ** $p < 0.01$; **** $p < 0.0001$; compared with *Syt1* cKO neurons – CRE. # $p < 0.05$; ## $p < 0.01$; ### $p < 0.001$; #### $p < 0.0001$; compared with *Syt1* cKO neurons + CRE.

ester of JF₆₄₆-BAPTA bearing a HaloTag ligand (JF₆₄₆-BAPTA-AM-HTL) (Deo et al., 2019), a gift from L. Lavis (Janelia Research Campus). After a 20 min incubation at 37°C, the cells were again washed with dye-free ACSF and incubated for 20 min at 37°C before being mounted in the imaging chamber; 5 FOV were selected per coverslip. Three seconds of baseline were recorded before a saturating stimulus (50 APs at 50 Hz) was delivered to establish a maximum fluorescence (F_{max}) for each FOV. At least 5 min elapsed between imaging each FOV to give the neurons time to recover and return to basal conditions.

Image analysis. For colocalization analysis, the Coloc2 plugin in Fiji (Schindelin et al., 2012) was used to determine the Mander’s overlap

coefficients and Pearson’s correlation coefficients; Costes’ automatic threshold regression was used for both determinations.

For synapse counting analysis, images were exported to SynD (Schmitz et al., 2011), where the image of MAP2 staining was used to create a neurite mask; then synaptic density was quantified by counting the number of overlapping VGAT and Gephyrin puncta within the neurite mask and dividing the total number by the length of dendrite measured to yield number of synapses per micron.

For SP-pH release analysis, Fiji with the DCV_pHluorin toolset (https://github.com/alemoro/DCVpHluorin_toolset) (Moro et al., 2021) was used; 3 pixels \times 3 pixels ROIs were placed over each observed increase in fluorescence, and somatic events were excluded. Fusion

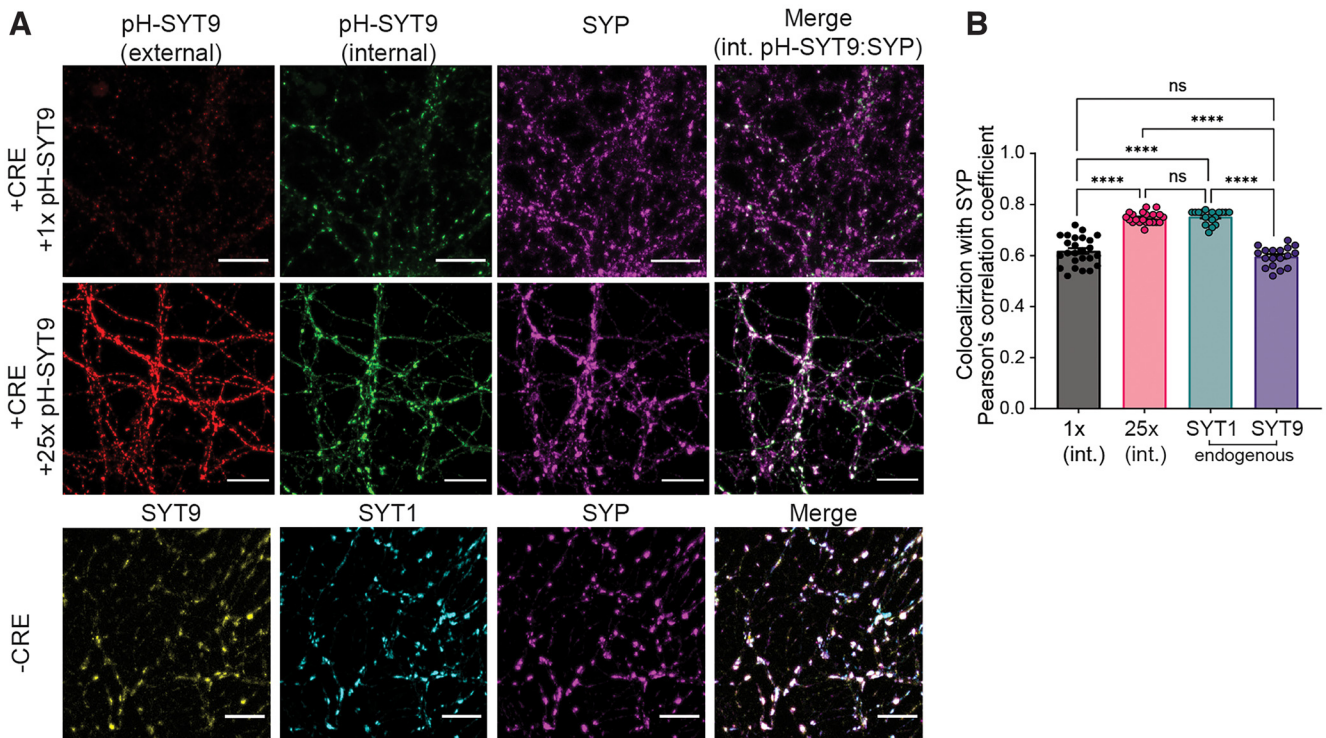


Figure 5. Overexpression of SYT9 leads to increased SV localization. **A**, Representative immunofluorescence images of cultured *Syt1* cKO cortical neurons \pm CRE, with and without overexpressed pH-SYT9. Rescue constructs were tagged at the N-terminus with a pHluorin to enable differential labeling of the surface and internal fractions using α -GFP antibodies (for details, see Materials and Methods). pH-SYT9 was present in both the plasma membrane (red) and on internal compartments (green). SVs were marked using an α -SYP antibody (magenta). **B**, Quantification of the colocalization between SYP and the following: 1 \times internal pH-SYT9 ($n = 25$, 0.618 ± 0.0112), 25 \times internal pH-SYT9 ($n = 21$, 0.747 ± 0.00484), endogenous SYT1 ($n = 18$, 0.752 ± 0.00613), and endogenous SYT9 ($n = 18$, 0.597 ± 0.00918) (one-way ANOVA $F = 86.69$, $R^2 = 0.7693$, $p < 0.0001$). Subsequent pairwise analyses with Tukey's multiple comparisons test resulted in significant p values for 1 \times (int.) versus 25 \times (int.) ($p < 0.0001$), 1 \times (int.) versus Endo SYT1 ($p < 0.0001$), Endo SYT9 versus 25 \times (int.) ($p < 0.0001$), and Endo SYT1 versus Endo SYT9 ($p < 0.0001$); all other comparisons yielded $p > 0.1$. **** $p < 0.0001$. ns, $p > 0.05$. Scale bars, 20 μ m.

events were defined as a sudden increase of 2 SDs above the average fluorescence of the first 100 frames in the ROI (F_0). Time-lapses were also manually scored along with the DCV_pHluorin analysis algorithm to ensure a thorough and complete characterization of each release event. Greater than 95% of ROIs contained only a single stepwise change in fluorescence after stimulation, so single ROIs were counted as single fusion events. The start of a fusion event was defined as the first frame with a signal that was at least twice the background noise (i.e., $2 \times$ the SD of F_0), and end of a fusion event was defined by the first frame below this threshold. Most ROIs that contained a release event also showed increases in fluorescence after NH_4Cl perfusion (see Fig. 9F), indicating incomplete release of SP-pH. Pool size estimations were calculated using the same rules used for fusion event detection, after perfusion with NH_4Cl . Analysis was blinded, and the number of fusion events, SP-pH vesicle pool size estimation, event duration, and fusion onset timing were all determined using DCV_pHluorin. Output data were processed in Excel and plotted using GraphPad Prism.

Ca^{2+} imaging analysis was performed as previously described (Bradberry and Chapman, 2022) with a modified ImageJ script taken from Vevea and Chapman (2020). Briefly, SYP-HaloTag-JF₆₄₆-BAPTA traces were background-subtracted, and ROIs were created based on a custom workflow to identify changes in fluorescence of the selected image series. An average intensity projection of prestimulus baseline frames was subtracted from a maximum intensity projection of the entire time-lapse. This result was duplicated and mean filtered using a rolling ball radius of 10 pixels. The mean filtered image was subtracted from the original result,

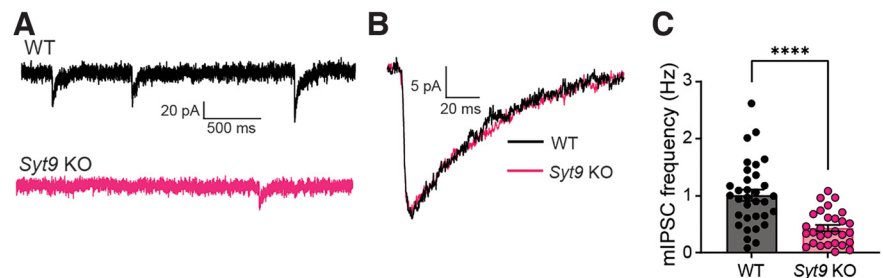


Figure 6. *Syt9* KO striatal neurons display decreased mIPSC frequency. **A**, Representative mIPSC traces recorded from WT ($n = 33$ neurons; 1.01 ± 0.0994 Hz) and *Syt9* KO ($n = 29$; 0.432 ± 0.0550 Hz) striatal neurons. **B**, Overlay of averaged mIPSCs from the two above conditions, revealing no change in kinetics or amplitude. **C**, mIPSC frequency is reduced in *Syt9* KO striatal neurons ($p < 0.0001$; Welch's t test $t = 5.082$, $df = 49.31$). **** $p < 0.0001$.

and this result was used to threshold changes in fluorescence. After thresholding, images were made binary, and a watershed function was run to separate overlapping objects. Using this procedure, objects (>10 pixels) were created and defined as ROIs. These ROIs were used to measure fluorescence changes over time from the original image series. The fluorescence traces of each ROI were then imported into AxoGraph where the basal, prestimulation fluorescence of each ROI (F_r) was subtracted from the max fluorescence at indicator saturation (F_{max}) to give a ΔF . The following equation was used to calculate presynaptic basal $[\text{Ca}^{2+}]_i$:

$$[\text{Ca}^{2+}]_i = K_D \left(\frac{F_r/F_{\text{max}} - 1/R_f}{1 - F_r/F_{\text{max}}} \right)^{1/n}$$

where K_D is the dissociation constant of the indicator, F_r is the baseline fluorescence of an ROI prestimulation, F_{max} is the fluorescence achieved

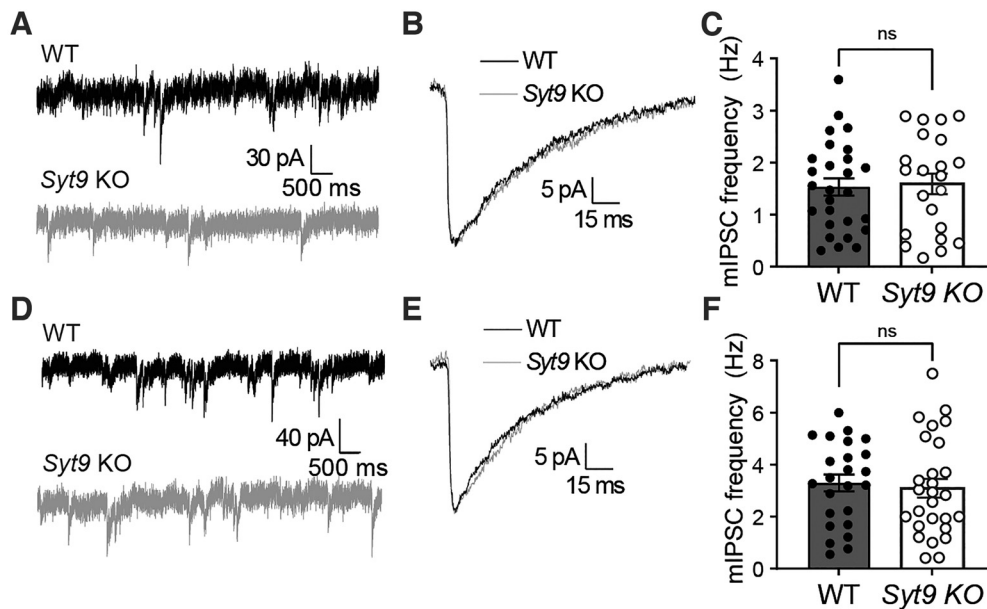


Figure 7. mIPSC frequency is unaltered in cultured *Syt9* KO cortical and hippocampal neurons. **A**, Representative mIPSC traces recorded from WT and *Syt9* KO cortical neurons. **B**, Overlay of averaged mIPSCs, revealing no apparent change in kinetics or amplitude. **C**, Average mIPSC frequency of WT ($n = 27$; 1.53 ± 0.166 Hz) and *Syt9* KO ($n = 27$; 1.59 ± 0.199 Hz) cortical neurons ($p = 0.8181$; unpaired t test; $t = 0.231$, $df = 47$). **D–F**, Same as **A–C**, but using hippocampal neurons (WT $n = 24$; 3.29 ± 0.325 Hz; KO $n = 27$; 3.09 ± 0.363 Hz) ($p = 0.684$; unpaired t test $t = 0.410$, $df = 49$).

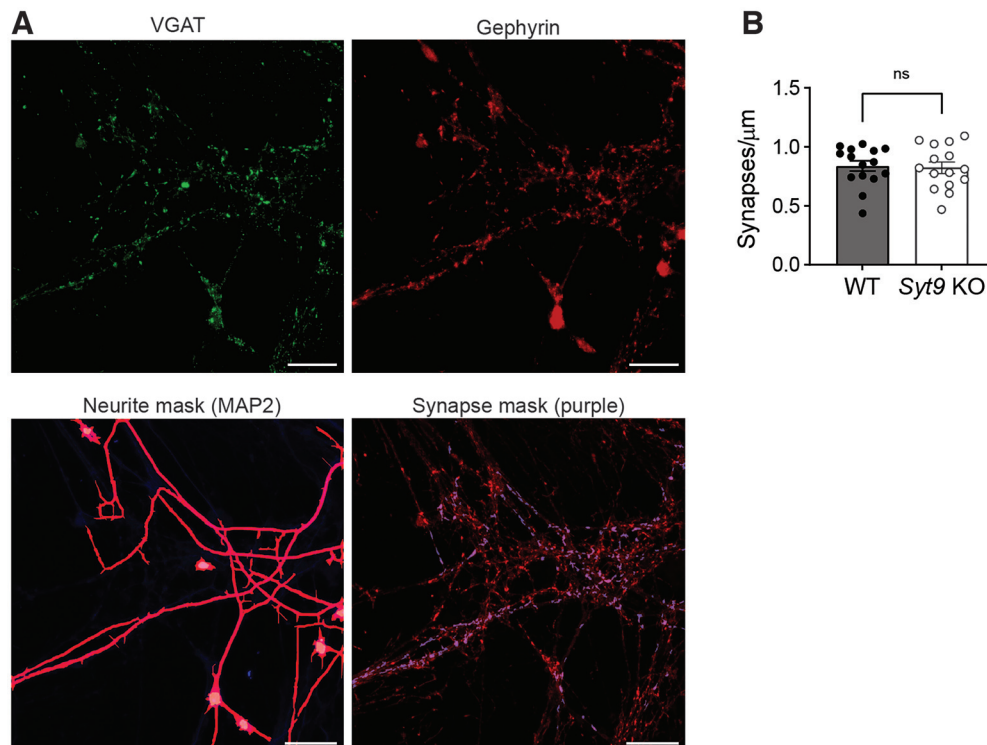


Figure 8. Unchanged synaptic density in *Syt9* KO striatal neurons. **A**, Representative images of cultured striatal neurons stained with α -Gephyrin (red) and α -VGAT (green) antibodies with a neurite mask generated from MAP2 staining (magenta). Gephyrin and VMAT overlap within the neurite mask were counted (purple puncta within synapse mask). Scale bars, $20 \mu\text{m}$. **B**, Number of synapses per micrometer is unaltered in cultured *Syt9* striatal neurons ($n = 15$; 0.823 ± 0.0476 synapses/ μm) compared with WT neurons ($n = 15$; 0.837 ± 0.0434 synapses/ μm) ($p = 0.8212$; unpaired t test $t = 0.228$, $df = 28$).

with the delivery of a saturating stimulus, R_f is the dynamic range of the indicator, and n is the Hill coefficient. For K_D , R_f and n , we used *in vitro* measurements ($K_D = 140$ nM, $R_f = 5.5$, $n = 1$) from (Deo et al., 2019).

Trafficking analysis was conducted using the Multi Kymograph plugin in Fiji; 30 s time-lapses, taken after NH_4Cl perfusion in the SP-pH

release experiments, were used; $90 \mu\text{m}$ segments that began within $20 \mu\text{m}$ of the soma were chosen. The kymograph was created from this time-lapse, and every path was traced and quantified.

Protein purification. Recombinant proteins were made as described previously (Evans et al., 2015). SYB2, SNAP-25B, and SYX were purified

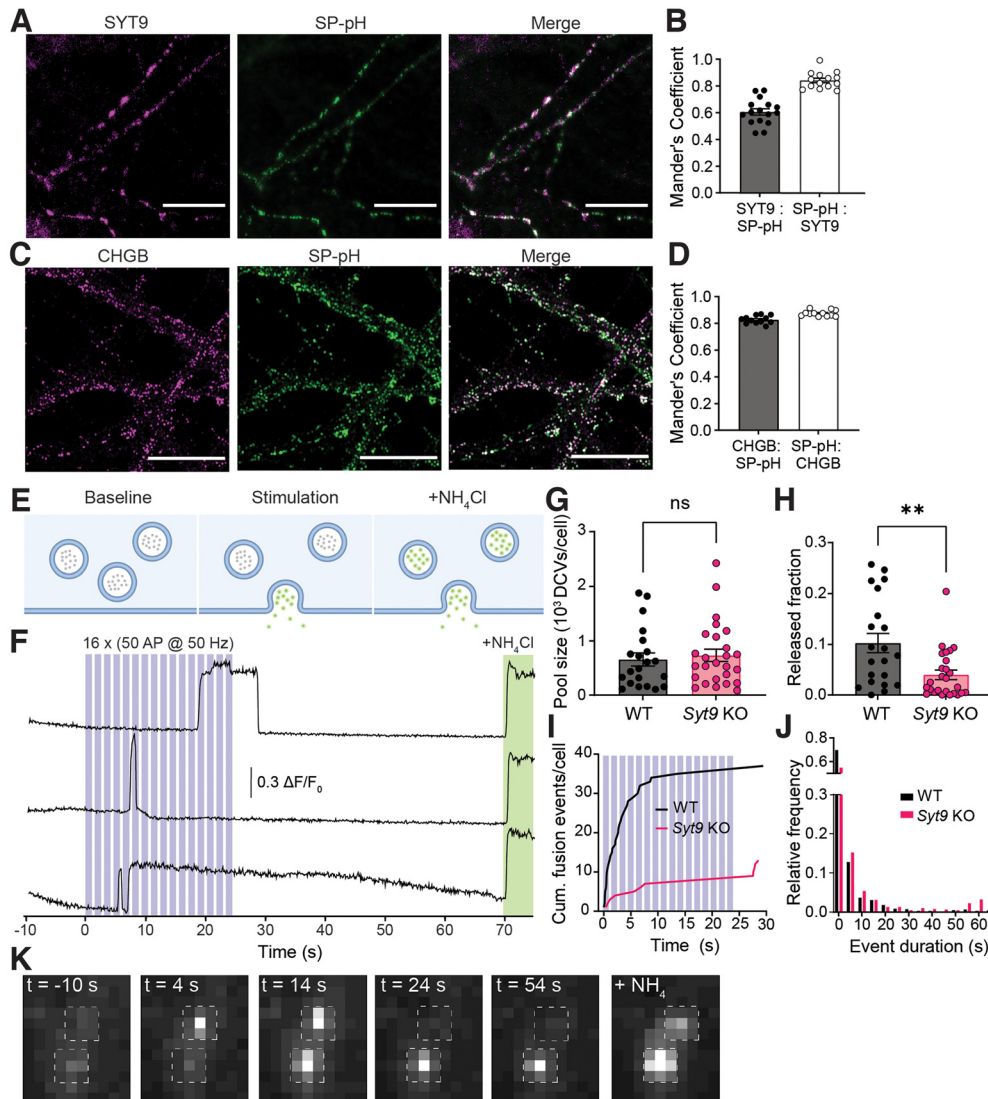


Figure 9. SYT9 regulates the secretion of SP-pHluorin from striatal neurons. **A**, Representative images of cultured striatal neurons stained with α -SYT9 (magenta) and α -GFP (SP-pH) (green) antibodies; channels are merged on the right. **B**, Quantification was conducted using the Mander's overlap coefficient; SYT9 overlaps with SP-pH to a higher degree (0.655 ± 0.0257), and SP-pH overlaps with SYT9 to a higher degree (0.808 ± 0.0174). **C**, **D**, Same as in **A**, **B**, but costained with α -CHGB (magenta) and α -GFP antibodies (green). SP-pH overlaps with CHGB to a high degree (0.855 ± 0.0118), and CHGB overlaps with SP-pH to a similar degree (0.881 ± 0.00755), confirming that SP-pH is targeted to DCVs. **E**, Schematic of the SP-pH release assay. **F**, Representative traces of individual SP-pH vesicle fusion events; the stimulation paradigm is overlaid in blue, and alkalization of DCVs with NH_4Cl is shown in green. **G**, Pool size per neuron was unchanged in *Syt9* KO neurons ($n = 27$ neurons; 731 ± 113 vesicles) compared with WT neurons ($n = 21$; 657 ± 120 vesicles) ($p = 0.6034$; Mann–Whitney $U = 248$). **H**, The released fraction of SP-pH is reduced in *Syt9* KO neurons ($n = 27$; 0.0398 ± 0.00926) compared with WT ($n = 21$; 0.103 ± 0.0189) ($p = 0.0049$; Mann–Whitney $U = 143.5$). **I**, Plot of cumulative SP-pH fusion events; again, the stimulus protocol is indicated in blue. **J**, Histogram of SP-pH release event duration for WT (median \pm SEM, 1.00 ± 0.290 s) and *Syt9* KO (median \pm SEM, 1.80 ± 0.614 s) striatal neurons. **K**, Representative ROIs in a time-lapse, demonstrating changes in SP-pH fluorescence over the course of an imaging experiment, taken from *Movie 1*; time points are indicated, with the stimulus at $t = 0$. The last image shows the same ROI after perfusion with NH_4Cl to neutralize the luminal pH of SP-pH-bearing DCVs, as indicated in **F**. ****** $p < 0.01$.

as His₆-tagged proteins using the pTrcHis vector. The SYT1 cytoplasmic domain (SYT1 C2AB, residues 96–421; the amino acid residues of the other SYT constructs are indicated in parentheses), SYT1 C2A (96–264), and SYT1 C2B (248–421) were purified as GST-tagged proteins using a pGEX vector. The SYT9 cytoplasmic domain (SYT9 C2AB, 104–386), SYT9 C2A (124–211), and SYT9 C2B (253–344) were purified as GST-tagged proteins using a pGEX vector. Isolated SYT9 C2A and C2B domains, harboring Ca²⁺ ligand mutations, were purified in the same manner at the WT C2 domains. Full-length SYT9 was purified as a His₆-SUMO-tagged protein using the pET28 vector.

Vesicle preparation. Protein-free liposomes, for cosedimentation assays, were generated by drying lipids (30% PE and 70% PC; 15% PS, 30% PE, and 55% PC; and 25% PS, 30% PE, and 45% PC) in chloroform, under a stream of nitrogen. The film was rehydrated and suspended by vortexing in 50 mM HEPES-NaOH, 100 mM NaCl, pH 7.4, and extruded

through 50 nm polycarbonate membranes to generate liposomes (Avanti Polar Lipids). SNARE-bearing vesicles, for *in vitro* fusion assays, were prepared as previously described (Bhalla et al., 2006). Lipid compositions were as follows: 15% PS, 27% PE, 55% PC, 1.5% N-dodecyl- β -D-maltese (NBD)-PE, and 1.5% Rho-PE for SYB2 vesicles, and 25% PS, 30% PE, and 45% PC for SYX1A vesicles.

In vitro fusion assays. Fusion assays between SYB2 and SYX1A vesicles were conducted using a scaled-down version of the referenced method (Bhalla et al., 2006). For split t-SNARE fusion assays, 1 μM of the cytoplasmic domain (C2AB) or 2 μM of isolated C2 domains, SYB2 vesicles, SYX1A vesicles, 0.2 mM EGTA, and 7 μM soluble SNAP-25B were incubated for 20 min at 37°C. Ca²⁺ (1 mM final free concentration) was added, and the reaction was monitored for an additional 60 min. NBD was added at the end of the experiment, to yield the maximum fluorescence signal. NBD donor fluorescence was monitored using a Synergy HT multi-detection microplate reader (Bio-Tek). Traces were

normalized to the first time point, and the maximum fluorescence signal, to determine the $\%F_{\max}$.

Cosedimentation assays. WT SYT9 C2A, C2B, or C2AB ($4 \mu\text{M}$) were combined with protein-free liposomes (1 mM total lipid; %PS as indicated in Fig. 13C) in 0.2 mM EGTA or 1 mM Ca^{2+} and incubated for 15 min at room temperature. Samples were then centrifuged in an Optima MAX-E tabletop ultracentrifuge (Beckman Coulter) at $184,000 \times g$ (65,000 rpm) for 45 min at 4°C . After centrifugation, the supernatant (S) and the pellet (P) were collected, and equal fractions were subjected to SDS-PAGE and Coomassie Blue staining. Bands were quantified by densitometry and plotted.

Isothermal titration calorimetry (ITC). WT and CLM forms of the isolated C2 domains of SYT9 were dialyzed overnight in ITC buffer (50 mM HEPES-NaOH, pH 7.4, 200 mM NaCl, and 10% glycerol) in the presence of Chelex-100 resin (Bio-Rad), to remove residual divalent cations. ITC buffer was subsequently filtered and used to make Ca^{2+} and protein dilutions. Heat of binding was measured, using a MicroCal iTC200 (Malvern Panalytical), at 25°C , in response to 20 injections of Ca^{2+} into the sample cell containing $100 \mu\text{M}$ protein. Heat of dilution was corrected by subtracting the signal that arises when Ca^{2+} is diluted into buffer. Data were analyzed using the “sequential binding site” model in the data software package.

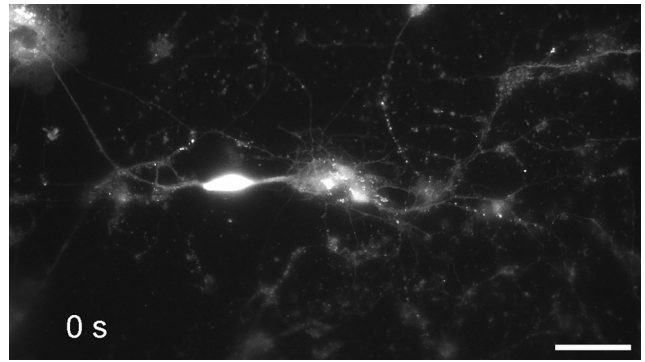
Experimental design and statistical analysis. Graphically, bars represent the mean and error bars indicate the SEM. For electrophysiological experiments and live-cell imaging experiments, each n represents a single neuron and n values were obtained from at least three separate animal preparations. All data were tested for normality with the D’Agostino & Pearson test; the appropriate statistical test was applied based on the reported normality of the data. All statistical tests were two-sided. Expected sample sizes were not estimated or predetermined. Statistical significance was assessed with two-tailed t tests, ANOVAs with *post hoc* pairwise comparisons, Mann–Whitney tests, or Kruskal–Wallis tests with *post hoc* pairwise comparisons as indicated in the text or legends. Specific values t , df , Mann–Whitney U , Kruskal–Wallis test statistic, p , and r^2 values are reported in the figure legends. All statistical analysis was conducted using GraphPad Prism 9.4 (GraphPad Software).

Results

SYT9 is not required for fast, synchronous neurotransmitter release in cultured neurons

Immunoblot analysis of neuronal culture lysates revealed that SYT1 and SYT9 are expressed in cortical, hippocampal, and striatal neurons (Fig. 1A,E). By including known amounts of purified recombinant SYT1 cytoplasmic domain (C2AB) or SYT9 (full-length) as standards on these blots, we were able to determine the absolute expression levels via quantitative densitometry (Fig. 1B,F). Briefly, recombinant protein standards were included in all immunoblots to generate standard curves. Ten micrograms of neuronal lysate protein were also immunoblotted, and the absolute levels of either SYT1 or SYT9 in the lysate were calculated from the standard curve in the same blot. This analysis revealed that SYT1 and SYT9 were $\sim 0.1\%$ and $\sim 0.004\%$ of the total protein in each of the neuronal lysates, respectively. Hence, SYT1 expression is ~ 25 times greater than SYT9 in all three classes of neurons.

A prior study suggested that SYT1 and SYT9 serve as partially redundant Ca^{2+} sensors in striatal neurons and that SYT9 can fully rescue fast release in *Syt1* KO cortical neurons (Xu et al., 2007). However, this is difficult to reconcile with the well-established findings that loss of SYT1 in hippocampal and cortical neurons disrupts virtually all synchronous release (Geppert et al., 1994; Maximov and Südhof, 2005). If SYT9 is a sensor for synchronous release, some fast release should have persisted in the *Syt1* KO neurons. To address this conundrum, whole-cell patch-



Movie 1. SYT9 regulates the secretion of SP-pH from striatal neurons. Representative time-lapse of SP-pH release events in a WT striatal neuron during electrical stimulation ($16 \times [50 \text{ AP at } 50 \text{ Hz}]$). Stimulation starts at $t = 10 \text{ s}$ and ends at $t = 34 \text{ s}$; NH_4 perfusion starts at $t = 80 \text{ s}$. Scale bar, $40 \mu\text{m}$. [View online]

clamp experiments were conducted using cultured neurons from *Syt1* cKO and *Syt9* KO mice. In striatal *Syt1* cKO neurons, ablation of SYT1 expression with application of CRE lentivirus eliminated fast, synchronous neurotransmitter release with an 8-fold reduction in evoked IPSC (eIPSC) amplitude (Fig. 1C,D). Disruption of SYT9 expression, however, did not result in any change in eIPSC amplitude or kinetics in striatal neurons (Fig. 1G,H). Analogous results were obtained using cultured cortical and hippocampal neurons (Fig. 2). Evoked release during a stimulus train was also unaffected in *Syt9* KO cortical, hippocampal, and striatal neurons, further demonstrating that this isoform does not impact evoked transmission (Fig. 3). We conclude that endogenous SYT9 is unable to support synchronous release in absence of SYT1 in any of the neuronal preparations studied here, perhaps because of the relatively low expression levels of this protein.

SYT9 rescues *Syt1* KO phenotypes only when overexpressed

Xu et al. (2007) reported that SYT9 overexpression can functionally rescue synchronous neurotransmitter release in cultured *Syt1* KO cortical neurons (Xu et al., 2007). Similar observations were made on overexpression of SYT9 in a calyx of Held slice preparation lacking the primary Ca^{2+} sensor at this synapse, SYT2 (Kochubey et al., 2016). Given the observation that endogenous SYT9 is expressed at levels ~ 25 -fold lower than SYT1 (Fig. 1B,F), a quantitative approach was taken to reevaluate this previously reported rescue activity. Cultured *Syt1* cKO cortical neurons were treated at DIV 1 with a CRE lentivirus to disrupt SYT1 expression and then transduced at DIV 5 with lentivirus to express SYT9 with an N-terminal pHluorin tag (pH-SYT9). The pH-SYT9 lentivirus was titered such that expression of pH-SYT9 in the + CRE neurons would be either $1 \times$ or $25 \times$ the endogenous SYT9 expression level, the latter condition matching the levels of endogenous SYT1 (Figs. 1, 4A). Ablation of SYT1 expression again resulted in a loss of fast, synchronous neurotransmission, and $1 \times$ overexpression of pH-SYT9 had no significant effect on eIPSC amplitude, and while there was a decrease in the time to peak this did not reach significance (Fig. 4B–E). However, $25 \times$ overexpression of pH-SYT9 significantly rescued the eIPSC amplitude (60% compared with – CRE) and completely rescued the eIPSC time to peak (Fig. 4B–E). The $25 \times$ overexpression condition also rescued the decay time of the + CRE condition (Fig. 4F). So, only supraphysiological SYT9 expression levels rescue evoked responses in neurons lacking SYT1 (Xu et al., 2007; Kochubey et al., 2016).

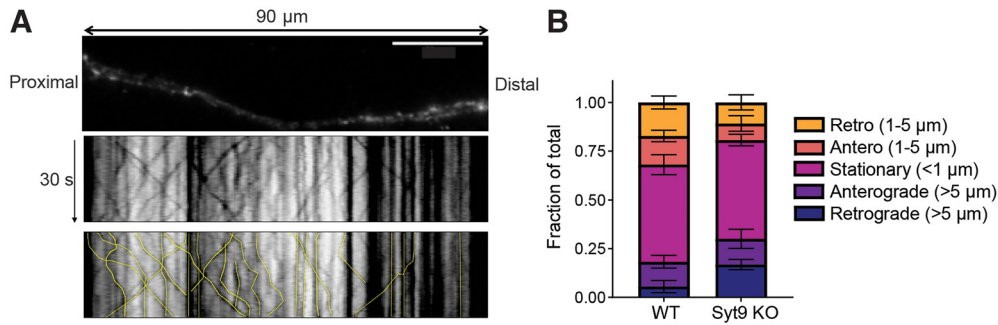


Figure 10. The trafficking of SP-pH-bearing DCVs is unaltered in *Syt9* KO striatal neurons. **A**, Top, Representative image of a 90 μm region of a striatal neuron transfected with SP-pH; image was captured after perfusion with NH₄Cl. Bottom panels, Color inverted kymographs of this region, over a 30 s time period; each track in the kymograph was traced and quantified in the bottom panel (yellow lines). **B**, Quantification of the displacement and direction of SP-pH vesicles. No significant differences were detected between WT ($n = 98$ vesicles, from 5 cells) versus *Syt9* KO ($n = 101$ vesicles, from 5 cells) striatal neurons (two-way ANOVA; $F_{(4,40)} = 1.903$, $p = 0.1289$).

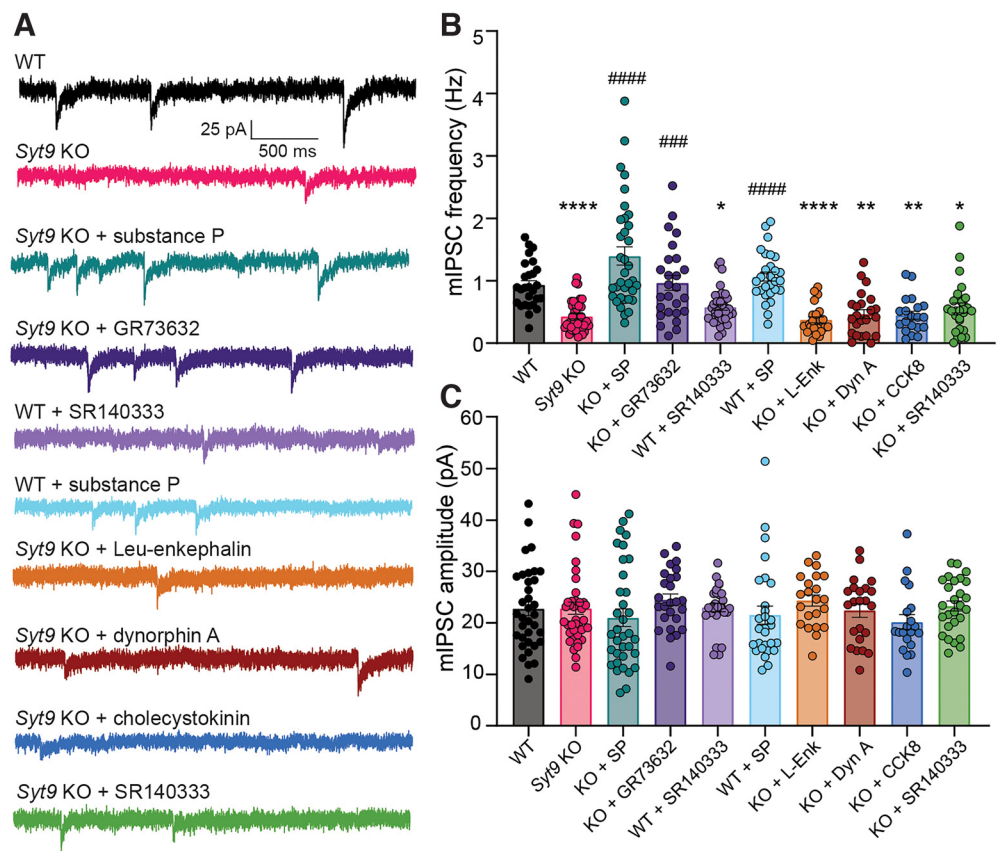


Figure 11. Treatment with SP rescues *Syt9* KO mIPSC phenotype. **A**, Representative mIPSC traces recorded from striatal neurons with measured mini frequencies as follows: WT ($n = 35$ neurons; 0.931 ± 0.0709 Hz); *Syt9* KO ($n = 39$; 0.430 ± 0.0385 Hz); WT with application of 100 nM SP ($n = 28$; 1.07 ± 0.0743 Hz) or 10 nM SR140333 ($n = 34$; 0.578 ± 0.0487 Hz); *Syt9* KO with application of 100 nM SP ($n = 35$; 1.40 ± 0.145 Hz), 100 nM GR73632 ($n = 26$; 0.967 ± 0.120 Hz), 10 nM SR140333 ($n = 27$; 0.564 ± 0.0795 Hz), 100 nM Leu-enkephalin ($n = 23$; 0.374 ± 0.0482 Hz), 100 nM dynorphin A ($n = 23$; 0.466 ± 0.0722 Hz), or 100 nM cholecystokinin ($n = 20$; 0.450 ± 0.0645 Hz) in the bath solution. **B**, Plot of average frequency of mIPSCs recorded from **A**; Kruskal–Wallis test $H = 111$, $p < 0.0001$. Subsequent pairwise analyses with Dunn’s multiple comparisons test resulted in significant p values for WT versus *Syt9* KO ($p < 0.0001$), WT versus WT + SR140333 ($p = 0.0322$), WT versus KO + L-Enk ($p < 0.0001$), WT versus KO + DynA ($p = 0.0013$), WT versus KO + CCK8 ($p = 0.0011$), WT versus KO + SR140333 ($p = 0.0133$), KO versus KO + SP ($p < 0.0001$), KO versus KO + GR73632 ($p = 0.0005$), and KO versus WT + SP ($p < 0.0001$); all other comparisons yielded $p > 0.999$. **C**, Plot of average mIPSC amplitudes for each condition; Kruskal–Wallis test $H = 16.55$, $p = 0.562$. * $p < 0.05$; ** $p < 0.01$; **** $p < 0.0001$; compared with WT neurons. ### $p < 0.001$; #### $p < 0.0001$; compared with *Syt9* KO neurons.

SYT1 is a multifunctional protein that also serves to clamp spontaneous neurotransmitter release under resting conditions (Liu et al., 2014; Bai et al., 2016; Courtney et al., 2019; Vevea and Chapman, 2020). To investigate whether overexpressed pH-SYT9 can clamp spontaneous fusion, mIPSCs (also called minis) were recorded in the presence of TTX, to block APs (Fig. 4G). Disruption of SYT1 resulted in an ~3-fold increase in mIPSC

frequency with no rescue observed in the 1× pH-SYT9 overexpression condition. In contrast, 25× overexpression of SYT9 resulted in a complete rescue of clamping activity (Fig. 4H). mIPSC amplitude was unaffected across conditions (Fig. 4I). Together, these findings indicate that SYT9 can rescue evoked release and clamp spontaneous release, in *Syt1* KO neurons, only when massively overexpressed.

To investigate how the localization of overexpressed SYT9 functions to support SV release, we used the N-terminal pHluorin tag to differentiate between pools in the plasma membrane versus internal compartments (see Materials and Methods) (Courtney et al., 2019). Briefly, before fixation and permeabilization, cultured neurons were incubated with a rabbit anti-GFP antibody to label all surface-resident pH-SYT9. Then, after fixation and permeabilization, the cultures were incubated in a chicken anti-GFP antibody to label all pH-SYT9 on internal compartments. Using different species of anti-GFP antibodies allowed for differential labeling by fluorescent secondary antibodies. We costained with antibodies against SYP to label SVs. The internal fraction in the 1× overexpression condition showed some degree of colocalization with SYP, and the internal fraction of 25× pH-SYT9 had a higher degree of colocalization. We note that endogenous SYT9 colocalized with SYP to a similar degree as 1× overexpressed pH-SYT9, while 25× overexpressed pH-SYT9 colocalized with SYP to a similar degree as endogenous SYT1 (Fig. 5). Overexpression of SYT9 results in a greater degree of colocalization with SYP, suggesting that some fraction of the overexpressed protein is targeted to SVs. This increased SV localization likely underlies the apparent rescue of both fast, synchronous neurotransmitter release and clamping of spontaneous release in *Syt1* KO neurons. So, while SYT9 has the intrinsic ability to regulate these aspects of SV release, it does so only after overexpression and mislocalization. These results are congruent with the idea that some SYT9 may be present on SVs, as indicated in proteomic studies (Takamori et al., 2006; Taoufiq et al., 2020). However, these levels are too low to support evoked release or to clamp spontaneous release, at least in the types of neurons studied here.

Decreased mIPSC frequency in *Syt9* KO striatal neurons

To further characterize neurotransmission in *Syt9* KO mice, spontaneous release from cultured striatal neurons was measured and compared with WT controls. We reiterate that all aspects of release evoked by single APs were normal (Fig. 1G); however, the mIPSC frequency in *Syt9* KO striatal neurons was reduced two-fold (Fig. 6A,C), with no effect on the amplitude or kinetics of these spontaneous quantal events (Fig. 6B). Interestingly, when the same experiment was performed using cortical and hippocampal neurons, loss of SYT9 did not affect spontaneous release rates (Fig. 7), suggesting that this phenotype was specific for striatal neurons, most of which are GABAergic medium spiny neurons (MSNs) (Kemp and Powell, 1971). Importantly, the density of synapses was unchanged between WT and *Syt9* KO striatal neurons (Fig. 8).

We note that most mIPSCs are Ca^{2+} -dependent and are thought to use the same Ca^{2+} sensors as evoked synchronous and asynchronous release, including SYT1 and Doc2 (Groffen et al., 2010; Courtney et al., 2018). The insufficiency of endogenous SYT9 to drive evoked release argues against the idea that it is a Ca^{2+} sensor for mIPSCs. Furthermore, the specificity of the mIPSC phenotype for striatal versus hippocampal or cortical neurons suggests a cell-specific mechanism for the action of SYT9 in spontaneous release. Notably, SYT9 is targeted to DCVs in a variety of tissues (Fukuda et al., 2002; Iezzi et al., 2005; Lynch and Martin, 2007; Roper et al., 2015), and some DCV neuropeptides have been shown to regulate aspects of synaptic transmission (Dean et al., 2009; Cao et al., 2011; He et al., 2019). This prompts the idea that SYT9 might regulate minis indirectly, potentially by controlling the release of neuromodulators from DCVs.

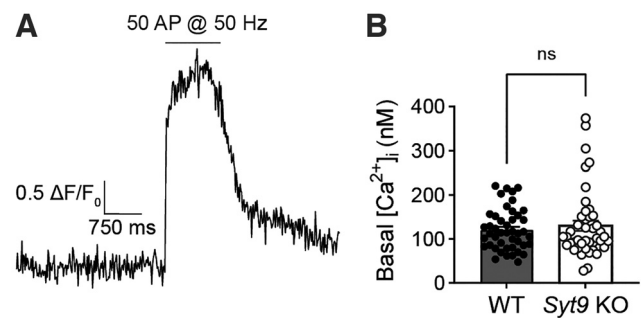


Figure 12. Basal presynaptic $[\text{Ca}^{2+}]_i$ is unchanged in *Syt9* KO striatal neurons. **A**, In each trial, the baseline signal was recorded for 3 s, followed by high-frequency train stimulation to obtain the maximal fluorescence of the indicator, to calculate the basal $[\text{Ca}^{2+}]_i$ (see Materials and Methods). **B**, Basal presynaptic $[\text{Ca}^{2+}]_i$ in 1.5 mM $[\text{Ca}^{2+}]_e$ did not differ between WT ($n = 45$; mean \pm SEM, 121 ± 6.99 nM) and *Syt9* KO ($n = 44$; mean \pm SEM, 130 ± 11.7 nM) striatal neurons ($p = 0.8735$; Mann–Whitney $U = 970$). ns, $p > 0.05$.

SYT9 regulates the secretion of SP-pHluorin from striatal neurons

To investigate the mechanism by which SYT9 regulates mIPSC frequency, we conducted further localization studies. Since the *Syt9* KO phenotype was specific for striatal neurons, we focused on striatum-specific DCV neuropeptides. Among these, SP was of particular interest because it has been shown to regulate mIPSC frequency in striatal neurons through its action on the neurokinin 1 receptor (NK1R) (He et al., 2019). Interestingly, SP is not enriched in hippocampal or cortical neurons (Shults et al., 1984), where the mIPSC phenotype was not observed.

Specific antibodies for SP are not available, so we transduced striatal neurons with a lentivirus that expresses an SP-pHluorin (SP-pH) fusion protein and performed immunocytochemistry to assess colocalization of the pHluorin tag with endogenous SYT9. Strikingly, SYT9 was colocalized with SP-pH (Fig. 9A,B). The correct localization of the SP-pH construct was confirmed by staining for CHGB, a canonical DCV marker in neurons (Fig. 9C,D). In summary, these findings demonstrate the presence of SYT9 on DCVs that bear a neuropeptide known to regulate mIPSC frequency (He et al., 2019).

Next, we sought to determine whether SYT9 regulates SP release from DCVs in striatal neurons. To optically measure SP secretion events at single-event resolution, WT and *Syt9* KO neurons were sparsely transfected with a plasmid encoding SP-pH along with a cytosolic mRuby construct to enable identification of transfected neurons and imaging of individual neurons within a network culture. SP-pH fluorescence is quenched in the low pH environment of the DCV lumen; on exocytosis, the pHluorin is rapidly dequenched, yielding a robust increase in fluorescence intensity (Fig. 9E). In cultured neurons, repetitive high-frequency electrical stimulation (i.e., 16 trains of 50 APs at 50 Hz) has been shown to effectively trigger these release events (Persoon et al., 2018); this paradigm was used in our experiments and yielded robust exocytosis (Fig. 9F; Movie 1). DCV fusion was quantified in WT and *Syt9* KO striatal neurons, where the released fraction was calculated as the number of fusion events divided by the total number of SP-pH vesicles in a single neuron. The total SP-pH DCV pool was estimated by perfusing neurons with NH_4Cl to alkalinize the lumen of DCVs and dequench the pHluorin reporter; no significant differences were observed between the WT and *Syt9* KO (Fig. 9G). In WT neurons, the released fraction was $\sim 10\%$. In *Syt9* KO neurons, this was reduced by $\sim 61\%$ (Fig. 9H,I), with only $\sim 3.9\%$ of the vesicles being released. Fusion event duration was also measured in

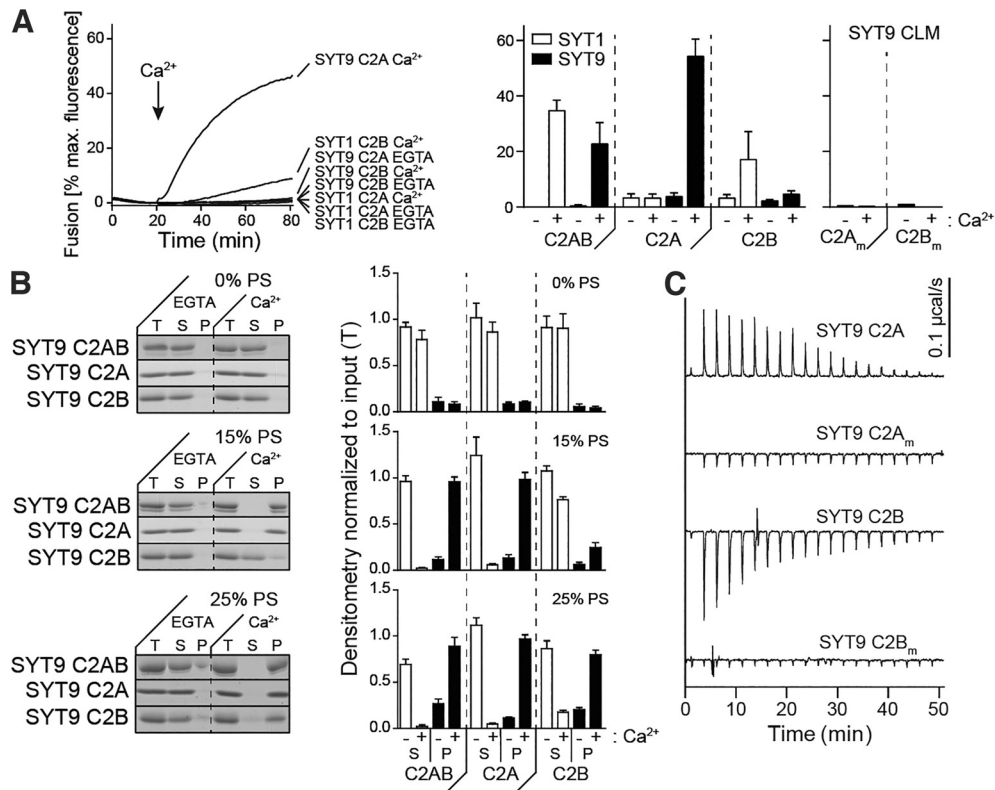


Figure 13. Ca²⁺•C2A from SYT9 regulates membrane fusion *in vitro*. **A**, Left, Reconstituted split t-SNARE fusion assay where Ca²⁺•SYT fragments must fold soluble SNAP-25B onto membrane-embedded SYX1A for fusion with SYB2 proteoliposomes to occur. Representative fusion traces, using each isolated C2 domain, C2A and C2B, from SYT1 and SYT9 are shown (left); the tandem C2 domains, C2AB, for each isoform were also assayed in parallel but were omitted for clarity. The isolated C2A domain, but not the C2B domain, of SYT9 stimulated fusion; in SYT1, C2B, rather than C2A, stimulated fusion (Gaffaney et al., 2008). Right, The extent of fusion (80 min), using all SYT constructs, in the presence (+) or absence (-) of Ca²⁺, is plotted ($n \geq 3$). **B**, Binding of SYT9 C2A, C2B, and C2AB to PS-bearing liposomes was monitored via a cosedimentation assay. Representative SDS-PAGE gels of protein from equal fractions of the supernatant (S), and pellet (P), as well as the total input (T), in the absence (0.2 mM EGTA) or presence of Ca²⁺ (1 mM free), using liposomes with 0%, 15%, and 25% PS, are shown (left). Protein band intensities were normalized to the total input and plotted (right; $n \geq 3$). **C**, Representative ITC traces showing the heat of Ca²⁺ binding to the isolated C2 domains of WT SYT9; the CLM domains (C2A_m and C2B_m) were analyzed in parallel, confirming that they fail to bind Ca²⁺ ($n = 4$ protein preparations). Thermodynamic values are provided in Table 1.

Table 1. Thermodynamic properties of Ca²⁺ binding to isolated C2 domains of SYT9 using ITC^a

	K_D (μM)	DH (cal/mol)	DS (cal/mol/K)	DG (kcal/mol)
SYT9 C2A	$K_{D1} = 53.0 \pm 8.6$	$DH_1 = 285 \pm 65$	$DS_1 = 20.6 \pm 0.49$	$DG_1 = -5.85 \pm 0.08$
	$K_{D2} = 182 \pm 39$	$DH_2 = 230 \pm 220$	$DS_2 = 18.0 \pm 1.1$	$DG_2 = -5.14 \pm 0.12$
	$K_{D3} = 337 \pm 80$	$DH_3 = 701 \pm 250$	$DS_3 = 18.5 \pm 0.50$	$DG_3 = -4.79 \pm 0.15$
SYT9 C2B	$K_{D1} = 42.9 \pm 5.5$	$DH_1 = -403 \pm 20$	$DS_1 = 18.7 \pm 0.30$	$DG_1 = -5.97 \pm 0.07$
	$K_{D2} = 500 \pm 95$	$DH_2 = -878 \pm 78$	$DS_2 = 12.3 \pm 0.58$	$DG_2 = -4.53 \pm 0.10$

^aThermodynamic properties of Ca²⁺ binding to the isolated C2A and C2B domains of SYT9 as determined using ITC. Representative traces of SYT9 C2 domain • Ca²⁺ titrations are shown in Figure 13C. Data are mean \pm SEM; $n = 4$.

WT and *Syt9* KO neurons, and there appeared to be a small population of long-duration release events that was absent in the WT (Fig. 9J), hinting at a potential role of SYT9 in regulating the fate of fusion pores, as shown for other SYT isoforms (Wang et al., 2001; Rao et al., 2014). Finally, loss of SYT9 had no apparent effect on the transport of SP-pH vesicles, suggesting that the observed reductions in SP secretion were not secondary to trafficking defects (Fig. 10).

Application of exogenous SP rescues the *Syt9* KO mIPSC phenotype

Since our data suggest that SYT9 regulates SP release (Fig. 9), and SP is known to modulate mIPSC frequency in striatal neurons (He et al., 2019), we sought to determine whether the *Syt9* KO phenotype could be rescued via acute application of this neuropeptide. In addition to SP, enkephalins, dynorphins, and

cholecystokinin are also enriched in the striatum (Krause et al., 1987; Angulo and McEwen, 1994), so we also assayed the effects of each of these neuropeptides (Fig. 11A). Acute addition of SP to the bath fully rescued the decreased mIPSC frequency in *Syt9* KO neurons. Rescue was also observed using GR73632, a synthetic NK1R agonist. In contrast, dynorphin A (DynA), Leu-enkephalin (L-Enk), and cholecystokinin (CCK8) had no effect, demonstrating that the mIPSC phenotype is SP-specific (Fig. 11B). Also, we found that SP supplementation did not significantly change the mIPSC frequency of WT neurons, indicating a high degree of SP-receptor activation under basal conditions.

Next, we further explored the SP-NK1R signaling pathway using a pharmacological approach. Application of SR140333, a synthetic NK1R antagonist (Jung et al., 1994), to WT neurons, phenocopied the *Syt9* KO; mIPSC frequency was reduced \sim 2-fold (Fig. 11B). This finding is consistent with a previous study

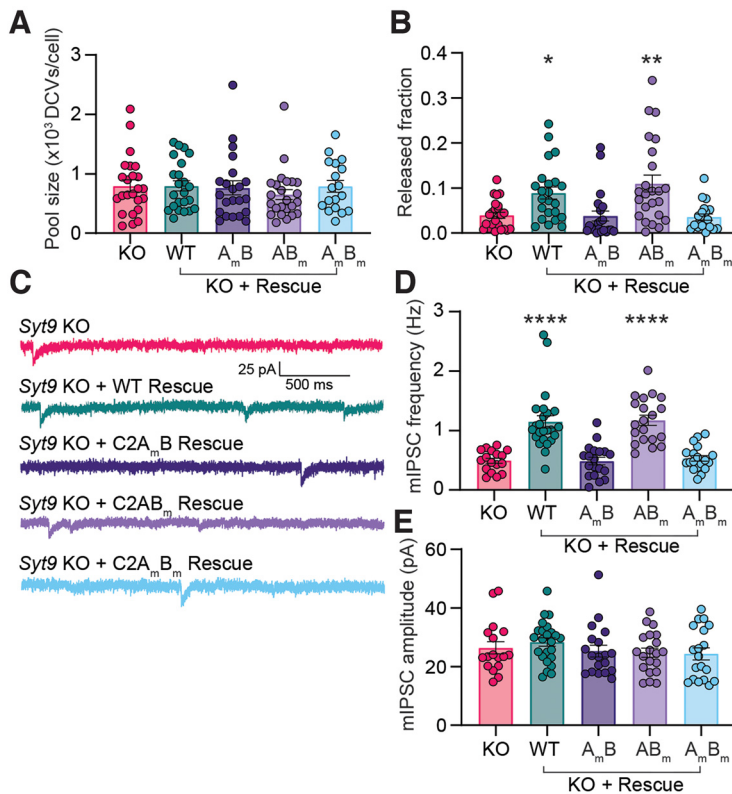


Figure 14. The Ca^{2+} binding activity of the C2A domain of SYT9 is required for its action in neurons. **A**, SP-containing DCV pool size was unchanged across *Syt9* KO rescue conditions ($p = 0.6272$; Kruskal–Wallis test $H = 2.598$). **B**, The reduction in SP-pH release in *Syt9* KO striatal neurons ($n = 21$ neurons; 0.0394 ± 0.00650) was rescued by expression of WT SYT9 ($n = 23$; 0.0889 ± 0.0132) or the C2A_mB mutant ($n = 24$; 0.110 ± 0.0187). In contrast, the C2A_mB ($n = 22$; 0.0382 ± 0.0112) and C2A_mB_m mutants ($n = 19$; 0.0356 ± 0.00712) both failed to rescue release (Kruskal–Wallis test $H = 27.65$; $p < 0.0001$). Subsequent pairwise analyses with Dunn’s multiple comparisons test resulted in significant p values for KO versus KO + WT ($p = 0.0158$) and KO versus KO + C2A_mB ($p = 0.0069$); all other comparisons yielded $p > 0.999$. Release was monitored as shown in Figure 9E–K. **C**, Representative mIPSC traces recorded from striatal neurons. **D**, Average frequency of mIPSCs recorded from **C** as follows: *Syt9* KO ($n = 17$; 0.493 ± 0.0434 Hz), *Syt9* KO + WT rescue ($n = 24$; 1.15 ± 0.103 Hz), *Syt9* KO + C2A_mB rescue ($n = 19$; 0.487 ± 0.0623 Hz), *Syt9* KO + C2A_mB_m rescue ($n = 20$; 1.17 ± 0.0856 Hz), and *Syt9* KO + C2A_mB_m rescue ($n = 19$; 0.531 ± 0.0473 Hz) (Kruskal–Wallis test $H = 57.16$, $p < 0.0001$). Subsequent pairwise analyses with Dunn’s multiple comparisons test resulted in significant p values for KO versus KO + WT ($p < 0.0001$) and KO versus KO + C2A_mB ($p < 0.0001$); all other comparisons yielded $p > 0.999$. **E**, mIPSC amplitudes measured from **C**. *Syt9* KO ($n = 17$; 26.4 ± 2.15 pA), *Syt9* KO + WT rescue ($n = 24$; 28.4 ± 1.45 pA), *Syt9* KO + C2A_mB rescue ($n = 19$; 25.3 ± 1.99 pA), *Syt9* KO + C2A_mB_m rescue ($n = 20$; 24.7 ± 1.59 pA), and *Syt9* KO + C2A_mB_m rescue ($n = 19$; 24.4 ± 2.02 pA). No significant differences in average amplitudes between conditions were observed (Kruskal–Wallis test $H = 3.92$, $p = 0.417$). Expression of WT SYT9 and the C2A_mB mutant in *Syt9* KO neurons rescued both SP release and the mini frequency phenotypes, while the C2A_m and C2A_mB_m mutants failed to rescue these phenotypes. * $p < 0.05$; ** $p < 0.01$; **** $p < 0.0001$; comparisons with the *Syt9* KO condition.

using a different NK1R antagonist (He et al., 2019), and confirms that the SP–NK1R pathway serves to regulate mini frequency in striatal neurons. Consistent with this model, SR140333 had no effect on mini frequency in *Syt9* KO neurons, presumably because of the large reduction in SP release from these cells and the concomitant decrease in NK1R activation. No differences in mIPSC amplitude were observed across all conditions (Fig. 11C). In summary, SYT9 regulates SP release, and activation of the NK1R by SP is pivotal in the regulation of mIPSCs in striatal neurons.

The binding of SP to the NK1 receptor presumably activates $G_{q/11}$, resulting in the generation of IP_3 and the mobilization of Ca^{2+} from internal stores. While basal presynaptic $[\text{Ca}^{2+}]_i$ did not appear to be altered in the *Syt9* KO striatal neurons (Fig. 12), it has been shown that local, transient increases in $[\text{Ca}^{2+}]_i$, mediated by IP_3 receptors in the presynaptic ER, drive spontaneous

neurotransmitter release in pyramidal neurons (Emptage et al., 2001; Simkus and Stricker, 2002). We therefore speculate that decreased SP-mediated IP_3 signaling in the *Syt9* KO underlies the decreased mIPSC phenotype observed in our studies.

Ca^{2+} binding to the C2A domain of SYT9 is crucial for its function *in vitro* and in neurons

The findings presented thus far suggest a model in which SYT9 regulates SP release which, in turn, modulates mini frequency. To further evaluate this model and directly determine whether SYT9 serves as a Ca^{2+} sensor for SP release, we sought to identify the structural elements in SYT9 that regulate membrane fusion *in vitro*, and then correlate these findings with the function of SYT9 in regulating both SP release and mini frequency. For these experiments, we used soluble, cytoplasmic fragments of SYT9, and for comparison, SYT1, in a “split t-SNARE” *in vitro* fusion assay (Bhalla et al., 2006) that mimics fusion of SVs with the plasma membrane in cells. In this assay, SYT fragments must first fold soluble SNAP-25B onto membrane-embedded SYX1A for fusion with SYB2-bearing liposomes to occur. Consistent with a previous study (Roper et al., 2015), the cytoplasmic domains (C2AB) of both SYT1 and SYT9 stimulated fusion to similar extents in the presence of Ca^{2+} (omitted for clarity in Fig. 13A, left, but quantified in Fig. 13A, right). We extended these experiments by evaluating the isolated C2 domains of each isoform and found that the C2A domain of SYT9 strongly stimulated fusion in response to Ca^{2+} , while C2B had little effect (Fig. 13A). This is in sharp contrast to SYT1, where C2B, but not C2A, facilitated fusion (Fig. 13A) (Gaffan et al., 2008). Additionally, we used CLMs, in which native Asp residues (D197, D199 in C2A and D330, D332 in C2B) that serve as conserved Ca^{2+} ligands in numerous isoforms were substituted with Asn, in either C2A or C2B of SYT9. These mutations disrupted the Ca^{2+} binding activity (Fig. 13C) of each C2 domain and abolished the ability of the C2A domain of SYT9 to stimulate membrane fusion in response to Ca^{2+} (Fig. 13A). Hence, these two related isoforms have diverged unexpectedly, with C2A serving as the primary Ca^{2+} sensing domain in SYT9, while C2B is more crucial in SYT1.

Since SYT1 regulates fusion via interactions with membranes that harbor anionic phospholipids (Bhalla et al., 2005; Liu et al., 2014; Bai et al., 2016), we assayed the ability of SYT9 to bind phosphatidylserine (PS)-harboring membranes in the presence and absence of Ca^{2+} . A previous study reported that for SYT9 C2A, but not C2B, bound to PS-bearing vesicles (Shin et al., 2004). We found that each of the isolated C2 domains efficiently bound to liposomes, in response to Ca^{2+} , when the mole fraction of PS was increased from 15% to 25%; this interaction is physiologically relevant since PS is $\sim 22\%$ of the inner leaflet of the plasma membrane (Hamilton et al., 2000) (Fig. 13B).

We also directly measured Ca^{2+} binding to the isolated C2 domains of SYT9, using ITC; calorimetry data for SYT1 have been previously reported (Radhakrishnan et al., 2009; Evans et al., 2016). Ca^{2+} binding to SYT9 C2A was endothermic, and binding to C2B was exothermic (Fig. 13C). When fitted with a sequential binding site model, C2A exhibited three binding sites with K_D values of 53, 182, and 337 μM ; C2B had two binding sites, with K_D values of 43 and 500 μM (for all thermodynamic values, see Table 1). Interestingly, the K_D value for the third binding site of C2A (337 μM) was significantly lower than the value reported for SYT1 ($K_D > 1 \text{ mM}$) (Radhakrishnan et al., 2009; Evans et al., 2016). Titrations were also performed on the CLM forms of isolated C2A or C2B, described above, and these constructs yielded little to no signal, confirming they fail to bind Ca^{2+} (Fig. 13C). These experiments demonstrate that while both isolated C2 domains bind Ca^{2+} , only C2A was able to effectively stimulate membrane fusion.

Next, if our model is correct, the biochemical results above suggest that Ca^{2+} binding to C2A, but not C2B, should underlie the ability of SYT9 to promote SP release. To test this, full-length variants of the SYT9 CLMs were generated and expressed in *Syt9* KO neurons via lentiviral transduction; WT SYT9 served as a positive control. SP release was monitored using the optical assay described in Figure 9. Importantly, full-length SYT9 constructs with mutated Ca^{2+} ligands in the C2A domain or both C2 domains, referred to as C2A_mB and C2A_mB_m, respectively, failed to rescue release, while the full-length construct with mutated Ca^{2+} ligands in the C2B domain, referred to as C2AB_m, exhibited full rescue (Fig. 14A) with no change in DCV pool size (Fig. 14B). Hence, the ability of these mutants to regulate reconstituted membrane fusion reactions *in vitro*, and to drive SP release from living neurons, were well correlated; in both cases, the C2A domain functioned as the crucial Ca^{2+} -sensing motif. These findings further support the idea that SYT9 functions as a Ca^{2+} sensor for DCV exocytosis.

Finally, we conducted patch-clamp recordings of *Syt9* KO striatal neurons that expressed each full-length CLM construct. Again, complete rescue of mIPSC frequency was observed using WT SYT9. In sharp contrast, SYT9 C2A_mB_m, which cannot bind Ca^{2+} via either C2 domain, failed to rescue the mini phenotype. Consistent with our model, C2A_mB also failed to rescue (Fig. 14C), while C2AB_m was as effective as the WT protein (Fig. 14D; no changes in mini amplitude were observed across conditions [Fig. 14E]). In summary, Ca^{2+} binding to the C2A domain, but not the C2B domain, underlies the ability of SYT9 to regulate membrane fusion to, in turn, indirectly control the rate of spontaneous release in striatal neurons by controlling SP secretion.

Discussion

SYT9 is widely expressed in the brain (Mittelstaedt et al., 2009) (these authors referred to SYT9 as SYT5), but KOs lacking this protein have only been characterized using the calyx of Held slice preparation (Kochubey et al., 2016) and cultured striatal neurons (Xu et al., 2007). SYT9 appears to be expressed in the calyx of Held, but loss of this protein did not affect AP-triggered neurotransmitter release (Kochubey et al., 2016). In contrast, in cultured striatal neurons, one study reported a 57% reduction in eIPSC amplitude in *Syt9* KO striatal neurons (Xu et al., 2007). However, this finding has not been reproduced, and it is difficult to reconcile with the expression patterns of SYT9 and SYT1. Namely, SYT9 is expressed at similar levels in cortical, hippocampal, and striatal neurons, and it is well established that loss of

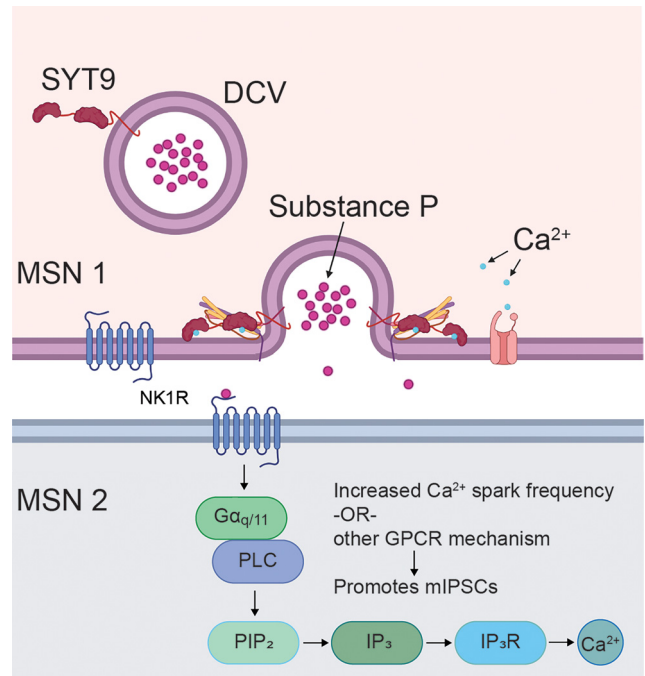


Figure 15. SYT9 indirectly controls mini frequency in striatal neurons by serving as a Ca^{2+} sensor for SP exocytosis. A model in which SYT9 serves as a Ca^{2+} sensor that regulates the exocytosis of SP-containing DCVs from striatal neurons. Released SP then activates the NK1 receptor, which in turn activates the IP₃ pathway via G_{q/11} and phospholipase C (PLC), leading to increased Ca^{2+} efflux from the ER, to promote spontaneous neurotransmitter release rates. SP likely acts in both a paracrine and an autocrine fashion; the signal transduction pathway in MSN 2 is also present in MSN 1 but was omitted for clarity.

SYT1 abolishes synchronous release in both cortical and hippocampal neurons (Geppert et al., 1994; Maximov and Südhof, 2005) (Fig. 1). So, it is apparent that endogenous SYT9 does not function as a Ca^{2+} sensor for synchronous SV exocytosis in either of these two classes of neurons (Figs. 1, 2). Here, we extended these observations to cultured striatal neurons and found that SYT1, but not endogenous SYT9, drives rapid SV exocytosis. We went on to show that SYT9 is largely localized to SP-bearing DCVs in striatal neurons, where it regulates the release of this neuropeptide to indirectly control mIPSC frequency. Evidently, at least some isoforms of SYT have become specialized to control the release of neuropeptides that impact synaptic function (Dean et al., 2009; Cao et al., 2011). It is tempting to speculate the divergence of numerous SYT isoforms might enable the differential release of myriad distinct neuromodulators and hormones, in response to different patterns of activity (Moghadam and Jackson, 2013).

We found that SYT9 is expressed at ~25-fold lower levels than SYT1 (Fig. 1). Given the estimate of ~15 copies of SYT1 per SV (Takamori et al., 2006), the abundance of SYT9 on SVs would, on average, be expected to be low, particularly since its primary localization appears to be on DCVs (Fig. 8). Some fraction of SYT9 does colocalize with canonical SV markers (Fig. 5) (Xu et al., 2007), and SYT9 was detected in proteomic studies of purified SVs (Takamori et al., 2006; Taoufiq et al., 2020) (these authors referred to SYT9 as SYT5). Thus, it remains possible that there could be limited populations of SVs, in discrete brain regions, which harbor a sufficient copy number of SYT9 molecules to trigger SV exocytosis. However, in our hands, this was not the case with cortical, hippocampal, or striatal neurons (Figs. 1, 2). It should also be emphasized that DCVs are often

present in or near presynaptic nerve terminals (Persoon et al., 2018; Radhakrishnan et al., 2021), and this can potentially exaggerate the presence of SYT9 on SVs as determined via immunocytochemistry.

While our experiments indicate that SYT9 functions as a Ca^{2+} sensor for SP release from striatal neurons, some degree of regulated release persisted in the KO (Fig. 9), suggesting that additional Ca^{2+} sensors are associated with SP-bearing DCVs. Indeed, SYT1 was present on SP-bearing DCVs purified from rabbit optic nerve (Berg et al., 2000). Additionally, in hippocampal neurons, SYT1 and SYT7 have both been implicated in DCV exocytosis (van Westen et al., 2021), suggesting multiple roles for these Ca^{2+} sensors. We also note that SYT4, which does not bind Ca^{2+} , negatively regulates the release of BDNF (Dean et al., 2009), and SYT10, which binds Ca^{2+} , positively regulates the secretion of IGF-1 from DCVs in neurons (Cao et al., 2011). Collectively, these findings, combined with the observations in the current study, support the idea that the SYTs have diverged, at least in part, to control different forms of DCV exocytosis (Dean et al., 2012). We also reiterate that the *Syt9* KO mIPSC phenotype appears to be specific for striatal neurons, which robustly express SP. The function of SYT9 in cortical and hippocampal neurons remains unknown. We speculate that it regulates the release of neuropeptides; a future goal is to address this issue via colocalization studies and by isolating and characterizing SYT9-bearing organelles from these classes of neurons.

The loss of SYT9 in striatal neurons results in a decrease in spontaneous neurotransmitter release (Fig. 6). Spontaneous release is thought to play an important role in synapse function and structure. For example, minis modulate excitability by regulating the tonic activity of postsynaptic receptors (M. A. Sutton et al., 2004, 2006) and maintaining postsynaptic receptor density (Ehlers et al., 2007). Spontaneous release also regulates dendritic protein synthesis to control aspects of synaptic plasticity (M. A. Sutton and Schuman, 2006). Further work is now needed to address how the change in mini frequency, in *Syt9* KO striatal neurons, affects their function and plasticity in native circuits.

Regarding the diversity of SYT isoforms, our finding that the C2A domain of SYT9 serves as the crucial Ca^{2+} -sensing motif for fusion was unexpected. SYT9 forms a clade with SYT1/2, and Ca^{2+} ligand mutations in the C2B domain of SYT1 clearly disrupt function (Nishiki and Augustine, 2004), while similar mutations in C2A have been reported to either have no effect (Fernández-Chacón et al., 2002), to be gain of function (Stevens and Sullivan, 2003; Pang et al., 2006b), or to cause partial loss of function (Shin et al., 2009). Moreover, the isolated C2B domain of SYT1, but not the C2A domain, regulates fusion *in vitro* (Fig. 13) (Gaffaney et al., 2008). In contrast, Ca^{2+} binding to the C2A domain of SYT9, but not the C2B domain, was required to both stimulate fusion *in vitro* (Fig. 13) and promote SP release from striatal neurons to regulate minis (Fig. 14). Apparently, this shuffling of C2 domain function is tolerated, as SYT9 can rescue evoked neurotransmitter release and clamp spontaneous release in *Syt1* KO neurons, when sufficiently overexpressed (Fig. 4).

Returning to the physiology, we emphasize that the striatum is a specialized structure with a dense local network largely composed of MSNs and their axon collaterals. While a substantial fraction of these neurons projects to other brain regions, direct synaptic communication between MSNs also occurs (Tunstall et al., 2002); this is the condition recapitulated in our experiments using cultured striatal neurons. Subpopulations of MSNs release SP within the striatum (Gerfen, 1992) and harbor NK1 receptors

(Haneda et al., 2007). We observed modulation of MSN-MSN transmission by SP in culture, and the next step will be to measure such modulation in acute striatal slice preparations. In addition, MSNs project to targets in the substantia nigra and globus pallidus, and recordings from brain slices that encompass the striatum along with these other structures will address the role of SYT9-regulated SP release at terminals that innervate these target cells. Moreover, SP enhances center-surround contrast of striosomal dopamine signals by modulating dopamine release from neurons that project from the substantia nigra onto striatal targets (Brimblecombe and Cragg, 2015). Hence, slice recordings, to measure dopamine release, are an important future direction of this work.

We propose that SP modulates spontaneous release rates in striatal neurons by binding the NK1 receptor and activating $\text{G}_{q/11}$, resulting in the generation of IP_3 and the mobilization of Ca^{2+} from internal stores (Fig. 15), thus increasing mini frequency. Indeed, localized increases in $[\text{Ca}^{2+}]_i$, mediated by IP_3 receptors in the presynaptic ER, have been reported to drive spontaneous release in pyramidal neurons (Emptage et al., 2001; Simkus and Stricker, 2002). A future goal is to compare these brief Ca^{2+} transients, akin to Ca^{2+} sparks in muscle cells, in WT and *Syt9* KO striatal neurons. Finally, we emphasize that the highest expression levels of SYT9 in mouse brain occur in the pituitary gland and hypothalamus, both of which are particularly rich sources of numerous classes of DCVs (Roper et al., 2015). It will be interesting to investigate whether SYT9 regulates the release of hypothalamic hormones.

References

- Angulo JA, McEwen BS (1994) Molecular aspects of neuropeptide regulation and function in the corpus striatum and nucleus accumbens. *Brain Res Rev* 19:1–28.
- Bai H, Xue R, Bao H, Zhang L, Yethiraj A, Cui Q, Chapman ER (2016) Different states of synaptotagmin regulate evoked versus spontaneous release. *Nat Commun* 7:10971.
- Berg EA, Johnson RJ, Leeman SE, Boyd N, Kimerer L, Fine RE (2000) Isolation and characterization of substance P-containing dense-core vesicles from rabbit optic nerve and termini. *J Neurosci Res* 62:830–839.
- Bhalla A, Tucker WC, Chapman ER (2005) Synaptotagmin isoforms couple distinct ranges of Ca^{2+} , Ba^{2+} , and Sr^{2+} concentration to SNARE-mediated membrane fusion. *Mol Biol Cell* 16:4755–4764.
- Bhalla A, Chicka MC, Tucker WC, Chapman ER (2006) Ca^{2+} -synaptotagmin directly regulates t-SNARE function during reconstituted membrane fusion. *Nat Struct Mol Biol* 13:323–330.
- Bhalla A, Chicka MC, Chapman ER (2008) Analysis of the synaptotagmin family during reconstituted membrane fusion: uncovering a class of inhibitory isoforms. *J Biol Chem* 283:21799–21807.
- Bradberry MM, Chapman ER (2022) All-optical monitoring of excitation-secretion coupling demonstrates that SV2A functions downstream of evoked Ca^{2+} entry. *J Physiol* 600:645–654.
- Brimblecombe KR, Cragg SJ (2015) Substance P weights striatal dopamine transmission differently within the striosome-matrix axis. *J Neurosci* 35:9017–9023.
- Cao P, Maximov A, Südhof TC (2011) Activity-dependent IGF-1 exocytosis is controlled by the Ca^{2+} -sensor synaptotagmin-10. *Cell* 145:300–311.
- Chapman ER (2008) How does synaptotagmin trigger neurotransmitter release? *Annu Rev Biochem* 77:615–641.
- Courtney NA, Briguglio JS, Bradberry MM, Greer C, Chapman ER (2018) Excitatory and inhibitory neurons utilize different Ca^{2+} sensors and sources to regulate spontaneous release. *Neuron* 98:977–991.e5.
- Courtney NA, Bao H, Briguglio JS, Chapman ER (2019) Synaptotagmin 1 clamps synaptic vesicle fusion in mammalian neurons independent of complexin. *Nat Commun* 10:4076.
- Craxton M (2010) A manual collection of *Syt*, *Esyt*, *Rph3a*, *Rph3al*, *Doc2*, and *Dblc2* genes from 46 metazoan genomes: an open access resource for neuroscience and evolutionary biology. *BMC Genomics* 11:37.

- Dean C, Liu H, Dunning FM, Chang PY, Jackson MB, Chapman ER (2009) Synaptotagmin-IV modulates synaptic function and long-term potentiation by regulating BDNF release. *Nat Neurosci* 12:767–776.
- Dean C, Dunning FM, Liu H, Bomba-Warczak E, Martens H, Bharat V, Ahmed S, Chapman ER (2012) Axonal and dendritic synaptotagmin isoforms revealed by a pHluorin-syt functional screen. *Mol Biol Cell* 23:1715–1727.
- Deo C, Sheu SH, Seo J, Clapham DE, Lavis LD (2019) Isomeric tuning yields bright and targetable red Ca²⁺ indicators. *J Am Chem Soc* 141:13734–13738.
- Ehlers MD, Heine M, Groc L, Lee MC, Choquet D (2007) Diffusional trapping of GluR1 AMPA receptors by input-specific synaptic activity. *Neuron* 54:447–460.
- Emptage NJ, Reid CA, Fine A (2001) Calcium stores in hippocampal synaptic boutons mediate short-term plasticity, store-operated Ca²⁺ entry, and spontaneous transmitter release. *Neuron* 29:197–208.
- Evans CS, He Z, Bai H, Lou X, Jeggle P, Sutton RB, Edwardson JM, Chapman ER (2016) Functional analysis of the interface between the tandem C2 domains of synaptotagmin-I. *Mol Biol Cell* 27:979–989.
- Evans CS, Ruhl DA, Chapman ER (2015) An engineered metal sensor tunes the kinetics of synaptic transmission. *J Neurosci* 35:11769–11779.
- Fernández-Alfonso T, Kwan R, Ryan TA (2006) Synaptic vesicles interchange their membrane proteins with a large surface reservoir during recycling. *Neuron* 51:179–186.
- Fernández-Chacón R, Shin OH, Königstorfer A, Matos MF, Meyer AC, Garcia J, Gerber SH, Rizo J, Südhof TC, Rosenmund C (2002) Structure/function analysis of Ca²⁺ binding to the C2A domain of synaptotagmin I. *J Neurosci* 22:8438–8446.
- Fukuda M, Kowalchuk JA, Zhang X, Martin TF, Mikoshiba K (2002) Synaptotagmin IX regulates Ca²⁺-dependent secretion in PC12 cells. *J Biol Chem* 277:4601–4604.
- Gaffaney JD, Dunning FM, Wang Z, Hui E, Chapman ER (2008) Synaptotagmin C2B domain regulates Ca²⁺-triggered fusion in vitro: critical residues revealed by scanning alanine mutagenesis. *J Biol Chem* 283:31763–31775.
- Geppert M, Goda Y, Hammer RE, Li C, Rosahl TW, Stevens CF, Südhof TC (1994) Synaptotagmin I: a major Ca²⁺ sensor for transmitter release at a central synapse. *Cell* 79:717–727.
- Gerfen CR (1992) The neostriatal mosaic: multiple levels of compartmental organization. *Trends Neurosci* 15:133–139.
- Groffen AJ, Martens S, Arazola RD, Cornelisse LN, Lozovaya N, Jong AP, Goriounova NA, Habets RL, Takai Y, Borst JG, Brose N, McMahon HT, Verhage M (2010) Doc2b is a high-affinity Ca²⁺ sensor for spontaneous neurotransmitter release. *Science* 327:1614–1618.
- Haberman Y, Grimberg E, Fukuda M, Sagi-Eisenberg R (2003) Synaptotagmin IX, a possible linker between the perinuclear endocytic recycling compartment and the microtubules. *J Cell Sci* 116:4307–4318.
- Hamilton J, Greiner R, Salem NJ, Kim HY (2000) n-3 fatty acid deficiency decreases phosphatidylserine accumulation selectively in neuronal tissues. *Lipids* 35:863–869.
- Haneda E, Higuchi M, Maeda J, Inaji M, Okauchi T, Ando K, Obayashi S, Nagai Y, Narazaki M, Ikehira H, Nakao R, Zhang MR, Suzuki K, Suzuki H, Suhara T (2007) In vivo mapping of substance P receptors in brains of laboratory animals by high-resolution imaging systems. *Synapse* 61:205–215.
- He ZX, Liu TY, Yin YY, Song HF, Zhu XJ (2019) Substance P plays a critical role in synaptic transmission in striatal neurons. *Biochem Biophys Res Commun* 511:369–373.
- Iezzi M, Eliasson L, Fukuda M, Wollheim CB (2005) Adenovirus-mediated silencing of Synaptotagmin 9 inhibits Ca²⁺-dependent insulin secretion in islets. *FEBS Lett* 579:5241–5246.
- Jung M, Calassi R, Maruani J, Barnouin M, Souilhac J, Poncelet M, Guedet C, Emondsalt X, Soubrié B, Brelière J, le Fur G (1994) Neuropharmacological characterization of SR 140333, a non peptide antagonist of NK1 receptors. *Neuropharmacology* 33:167–179.
- Kemp JM, Powell TP (1971) The structure of the caudate nucleus of the cat: light and electron microscopy. *Philos Trans R Soc Lond B Biol Sci* 262:383–401.
- Kochubey O, Babai N, Schneggenburger R (2016) A synaptotagmin isoform switch during the development of an identified CNS synapse. *Neuron* 90:984–999.
- Krause JE, Chirgwin JM, Carter MS, Xu ZS, Hershey AD (1987) Three rat preprotachykinin mRNAs encode the neuropeptides substance P and neurokinin A. *Proc Natl Acad Sci USA* 84:881–885.
- Kügler S, Kilic E, Bähr M (2003) Human synapsin 1 gene promoter confers highly neuron-specific long-term transgene expression from an adenoviral vector in the adult rat brain depending on the transduced area. *Gene Ther* 10:337–347.
- Ladner CL, Yang J, Turner RJ, Edwards RA (2004) Visible fluorescent detection of proteins in polyacrylamide gels without staining. *Anal Biochem* 326:13–20.
- Liu H, Bai H, Xue R, Takahashi H, Edwardson JM, Chapman ER (2014) Linker mutations reveal the complexity of synaptotagmin 1 action during synaptic transmission. *Nat Neurosci* 17:670–677.
- Lois C, Hong EJ, Pease S, Brown EJ, Baltimore D (2002) Germline transmission and tissue-specific expression of transgenes delivered by lentiviral vectors. *Science* 295:868–872.
- Lynch KL, Martin TF (2007) Synaptotagmins I and IX function redundantly in regulated exocytosis but not endocytosis in PC12 cells. *J Cell Sci* 120:617–627.
- Maximov A, Südhof TC (2005) Autonomous function of synaptotagmin 1 in triggering synchronous release independent of asynchronous release. *Neuron* 48:547–554.
- Miesenböck G, de Angelis DA, Rothman JE (1998) Visualizing secretion and synaptic transmission with pH-sensitive green fluorescent proteins. *Nature* 394:192–195.
- Mittelsteadt T, Seifert G, Álvarez-Barón E, Steinhäuser C, Becker AJ, Schoch S (2009) Differential mRNA expression patterns of the synaptotagmin gene family in the rodent brain. *J Comp Neurol* 512:514–528.
- Moghadam PK, Jackson MB (2013) The functional significance of synaptotagmin diversity in neuroendocrine secretion. *Front Endocrinol (Lausanne)* 4:124.
- Moro A, Hoogstraaten RI, Persoon CM, Verhage M, Toonen RF (2021) Quantitative analysis of dense-core vesicle fusion in rodent CNS neurons. *STAR Protoc* 2:100325.
- Nishiki TI, Augustine GJ (2004) Dual roles of the C2B domain of synaptotagmin I in synchronizing Ca²⁺-dependent neurotransmitter release. *J Neurosci* 24:8542–8550.
- Pang ZP, Melicoff E, Padgett D, Liu Y, Teich AF, Dickey BF, Lin W, Adachi R, Südhof TC (2006a) Synaptotagmin-2 is essential for survival and contributes to Ca²⁺ triggering of neurotransmitter release in central and neuromuscular synapses. *J Neurosci* 26:13493–13504.
- Pang ZP, Shin OH, Meyer AC, Rosenmund C, Südhof TC (2006b) A gain of function mutation in synaptotagmin-1 reveals a critical role of Ca²⁺-dependent soluble N-ethylmaleimide-sensitive factor attachment protein receptor complex binding in synaptic exocytosis. *J Neurosci* 26:12556–12565.
- Persoon CM, Moro A, Nassal JP, Farina M, Broeke JH, Arora S, Dominguez N, Weering JR, Toonen RF, Verhage M (2018) Pool size estimations for dense-core vesicles in mammalian CNS neurons. *EMBO J* 37:e99672.
- Quadros RM, et al. (2017) Easi-CRISPR: a robust method for one-step generation of mice carrying conditional and insertion alleles using long ssDNA donors and CRISPR ribonucleoproteins. *Genome Biol* 18:1–15.
- Radhakrishnan A, Stein A, Jahn R, Fasshauer D (2009) The Ca²⁺ affinity of synaptotagmin 1 is markedly increased by a specific interaction of its C2B domain with phosphatidylinositol 4,5-bisphosphate. *J Biol Chem* 284:25749–25760.
- Radhakrishnan A, Li X, Grushin K, Krishnakumar SS, Liu J, Rothman JE (2021) Symmetrical arrangement of proteins under release-ready vesicles in presynaptic terminals. *Proc Natl Acad Sci USA* 118:e2024029118.
- Rao TC, Passmore DR, Peleman AR, Das M, Chapman ER, Anantharam A (2014) Distinct fusion properties of synaptotagmin-1 and synaptotagmin-7 bearing dense core granules. *Mol Biol Cell* 25:2416–2427.
- Rickman C, Craxton M, Osborne S, Davletov B (2004) Comparative analysis of tandem C2 domains from the mammalian synaptotagmin family. *Biochem J* 378:681–686.
- Roper LK, Briguglio JS, Evans CS, Jackson MB, Chapman ER (2015) Sex-specific regulation of follicle-stimulating hormone secretion by synaptotagmin 9. *Nat Commun* 6:1–10.
- Schindelin J, Arganda-Carreras I, Frise E, Kaynig V, Longair M, Pietzsch T, Preibisch S, Rueden C, Saalfeld S, Schmid B, Tinevez JY, White DJ, Hartenstein V, Eliceiri K, Tomancak P, Cardona A (2012) Fiji: an open-source platform for biological-image analysis. *Nat Methods* 9:676–682.

- Schmitz SK, Hjorth JJ, Joemai RM, Wijntjes R, Eijgenraam S, de Bruijn P, Georgiou C, de Jong AP, van Ooyen A, Verhage M, Cornelisse LN, Toonen RF, Veldkamp W (2011) Automated analysis of neuronal morphology, synapse number and synaptic recruitment. *J Neurosci Methods* 195:185–193.
- Shin OH, Maximov A, Lim BK, Rizo J, Südhof TC (2004) Unexpected Ca^{2+} binding properties of synaptotagmin 9. *Proc Natl Acad Sci USA* 101:2554–2559.
- Shin OH, Xu J, Rizo J, Südhof TC (2009) Differential but convergent functions of Ca^{2+} binding to synaptotagmin-1 C2 domains mediate neurotransmitter release. *Proc Natl Acad Sci USA* 106:16469–16474.
- Shults CW, Quirion R, Chronwall B, Chase TN, O'Donohue TL (1984) A comparison of the anatomical distribution of substance P and substance P receptors in the rat central nervous system. *Peptides* 5:1097–1128.
- Simkus CR, Stricker C (2002) The contribution of intracellular calcium stores to mEPSCs recorded in layer II neurones of rat barrel cortex. *J Physiol* 545:521–535.
- Stevens CF, Sullivan JM (2003) The synaptotagmin C2A domain is part of the calcium sensor controlling fast synaptic transmission. *Neuron* 39:299–308.
- Sutton MA, Schuman EM (2006) Dendritic protein synthesis, synaptic plasticity, and memory. *Cell* 127:49–58.
- Sutton MA, Wall NR, Aakalu GN, Schuman EM (2004) Regulation of dendritic protein synthesis by miniature synaptic events. *Science* 304:1979–1983.
- Sutton MA, Ito HT, Cressy P, Kempf C, Woo JC, Schuman EM (2006) Miniature neurotransmission stabilizes synaptic function via tonic suppression of local dendritic protein synthesis. *Cell* 125:785–799.
- Sutton RB, Davletov BA, Berghuis AM, Südhof TC, Sprang SR (1995) Structure of the first C2 domain of synaptotagmin I: a novel Ca^{2+} /phospholipid binding fold. *Cell* 80:929–938.
- Takamori S, et al. (2006) Molecular anatomy of a trafficking organelle. *Cell* 127:831–846.
- Taoufiq Z, Ninov M, Villar-Briones A, Wang HY, Sasaki T, Roy MC, Beauchain F, Mori Y, Yoshida T, Takamori S, Jahn R, Takahashi T (2020) Hidden proteome of synaptic vesicles in the mammalian brain. *Proc Natl Acad Sci USA* 117:33586–33596.
- Tunstall MJ, Oorschot DE, Kean A, Wickens JR (2002) Inhibitory interactions between spiny projection neurons in the rat striatum. *J Neurophysiol* 88:1263–1269.
- van Westen R, Poppinga J, Díez Arazola R, Toonen RF, Verhage M (2021) Neuromodulator release in neurons requires two functionally redundant calcium sensors. *Proc Natl Acad Sci USA* 118:1–12.
- Vevea JD, Chapman ER (2020) Acute disruption of the synaptic vesicle membrane protein synaptotagmin 1 using knockoff in mouse hippocampal neurons. *Elife* 9:1–24.
- Wang CT, Grishanin R, Earles CA, Chang PY, Martin TF, Chapman ER, Jackson MB (2001) Synaptotagmin modulation of fusion pore kinetics in regulated exocytosis of dense-core vesicles. *Science* 294:1111–1115.
- Wolfes AC, Dean C (2020) The diversity of synaptotagmin isoforms. *Curr Opin Neurobiol* 63:198–209.
- Xu J, Mashimo T, Südhof TC (2007) Synaptotagmin-1, -2, and -9: Ca^{2+} sensors for fast release that specify distinct presynaptic properties in subsets of neurons. *Neuron* 54:567–581.